bioRxiv preprint doi: https://doi.org/10.1101/305441; this version posted April 24, 2018. The copyright holder for this preprint (which was not certified by peer review) is the author/funder, who has granted bioRxiv a license to display the preprint in perpetuity. It is made available under aCC-BY-NC-ND 4.0 International license.

Classification: Biological Sciences

Title: Autotransporter secretion exploits the bacterial actin-homologue

Mahmoud M. Ashawesh, Robert Markus, Christopher N. Penfold and Kim R. Hardie*

School of life Sciences, Centre for Biomolecular Sciences, University of Nottingham, University Park, NG7 2RD

***Corresponding Author:** Kim R Hardie, School of life Sciences, Centre for Biomolecular Sciences, University of Nottingham, University Park, NG7 2RD. Email kim.hardie@nottingham.ac.uk Tel 0115 8467958

Short Title: Autotransporter secretion exploits MreB and Sec

Key words: Autotransporter, Sec, MreB, bacterial cytoskeleton, protein secretion, super resolution microscopy

Abstract

Bacterial infection of humans, animals and plants relies heavily on secreted proteases that degrade host defences or activate bacterial toxins. The largest family of proteins secreted by Gram-negative pathogenic bacteria, the Autotransporters (ATs), includes key proteolytic virulence factors. There remains uncertainty about the mechanistic steps of the pathway ATs share to exit bacteria, and how it is energetically driven. This study set out to shed light on the AT secretion pathway with the ultimate aim of uncovering novel antimicrobial targets that would be unlikely to trigger the development of resistance mechanisms in bacteria. To do this, two AT virulence factors with distinct proteolytic functions, EspC (secreted from Enteropathogenic *Escherichia coli*) and AaaA (tethered to the extracellular surface of *Pseudomonas aeruginosa*) were chosen. EspC and AaaA were fluorescently labelled using two separate methods to establish the localization patterns of ATs as they are secreted from a bacterial cell. Super resolution microscopy revealed that localization of ATs occurs via a helical route along the bacterial cytoskeleton. In addition to requiring the conserved C-terminal β-barrel translocator domain of the AT, we present the first evidence that secretion is dependent on a dynamic interaction with a structure reliant upon the actin homologue MreB and the Sec translocon. These findings provide a step forward in the mechanistic understanding of the secretion of this widely distributed

bioRxiv preprint doi: https://doi.org/10.1101/305441; this version posted April 24, 2018. The copyright holder for this preprint (which was not certified by peer review) is the author/funder, who has granted bioRxiv a license to display the preprint in perpetuity. It is made available under aCC-BY-NC-ND 4.0 International license.

family of proteins that have pivotal roles in bacterial pathogenesis and conserved structural properties that could serve as novel broad-range antimicrobial targets.

Significance

Secreted bacterial proteases facilitate the infection of human, animal and plant hosts by degrading host defences or activating bacterial toxins. The autotransporter family is the largest family of proteins secreted from Gram-negative bacteria, and includes proteolytic virulence factors crucial to bacterial infection. Precisely how autotransporters migrate from the inside to the outside of the cell, and how this movement is energetically driven is a mystery. We demonstrate a spiral pathway of autotransporter secretion, presenting evidence that it involves a dynamic interaction with the actin homologue MreB that comprises the bacterial cytoskeleton. Our findings open the way to unravelling the mechanism of autotransporter secretion and offer the possibility to identify novel antimicrobial targets unlikely to trigger the development of antimicrobial resistance.

Introduction

Infections caused by Gram-negative bacteria are a major threat to the health of humans, plants and animals. The widely distributed autotransporter (AT) family includes numerous virulence factors that are vital to the pathogenicity of Gram-negative bacteria. ATs bear conserved structural features offering an ideal target for novel broad spectrum antimicrobials. Novel antimicrobial agents are desperately needed because those currently available have become less effective due to the emergence of antibiotic resistance in hospitals and communities (1,2). Virulence factors are only required during host infection offering targets less likely to trigger the development of resistance mechanisms in the bacteria (3). Since ATs are extracellular they are easily accessible to antimicrobials. Moreover, the AT secretion pathway offers an ideal target for novel antimicrobials (4-7) as it includes targets unique to bacteria that can be either narrow or broad spectrum (8).

Although the main steps of AT secretion have been identified, many mechanistic details remain unresolved and are hotly debated (7,9,10). What at first appeared a self-sufficient secretion pathway has since been shown to comprise of multiple components including the inner membrane (IM) Sec translocon, periplasmic chaperones and the outer membrane (OM) β-barrel assembly machinery (BAM) complex or two-membrane spanning complex TAM (Translocation and assembly module). How and where these components interact together to drive secretion remains to be elucidated, and could have a bearing on

bioRxiv preprint doi: https://doi.org/10.1101/305441; this version posted April 24, 2018. The copyright holder for this preprint (which was not certified by peer review) is the author/funder, who has granted bioRxiv a license to display the preprint in perpetuity. It is made available under aCC-BY-NC-ND 4.0 International license.

the overall building of the bacterial cell envelope because of the pleiotropic roles of the machineries involved. ATs bear 3 distinct domains: (i) the Sec-dependent signal sequence, that is located at the N-terminus, directs the secretion of the precursor across the IM; (ii) the central passenger domain that carries the functional site; and (iii) the carboxy terminal transporter domain, that inserts as a β-barrel into the OM and facilitates transport across the OM (10-13).

ATs function as adhesins (e.g. Ag43 of *Escherichia coli*) (14), toxins (e.g. VacA of *Helicobacter pylori*) (15), esterases (e.g. EstA of *Pseudomonas aeruginosa*) (16) and proteases (e.g. the Arginine-specific Aminopeptidase of *P. aeruginosa*, AaaA (17), and the serine protease of Enteropathogenic *E. coli* (EPEC), EspC (18)). The passenger domain of some ATs, e.g. EspC, is autoproteolytically cleaved internally and released externally (19). Other ATs, e.g. AaaA remain tethered to the outer membrane of the producing bacterium by their β-barrel, with the passenger domain exposed to the external milieu (17).

During their export to the outer membrane, several ATs have been detected at the bacterial pole (20). This localization is dependent on factors including (i) functional lipopolysaccharide (LPS) (20), (ii) the *E. coli* cytoplasmic chaperone DnaK (21), and (iii) a conserved cell division component FtsQ (22). The bacterial actin homologue (MreB) is the main component of the bacterial cytoskeleton (23,24) which influences chromosome segregation and cell polarity in addition to maintaining cell shape (25,26). The bacterial cytoskeleton is helical, with MreB forming cytoplasmic filaments which dynamically rotate around the cell circumference along the long axis in a manner reliant on the cell wall synthesis machinery (27). It has been suggested that the MreB cytoskeleton could act as a scaffold to provide paths for membrane protein localization and diffusion (28). In support of this, defects in MreB synthesis caused mislocalization of the type IV pilus retraction ATPase, PilT, away from bacterial poles of *P. aeruginosa* mutant strains (28), and disturbance in the localization of the AT IcsA and several polarized proteins in *Caulobacter crescentus* (29). In addition, MreB filaments have been implicated in the polar localization of aspartate chemoreceptor, Tar, leading us to speculate that polar localization of ATs could utilize MreB.

Despite lacking a typical Sec-targeting signal peptide, localization of MreB is dependent on the Sec system (30) revealing a previously unrecognized role of Sec in organizing bacterial cells on both sides of the IM. Moreover, Sec translocon proteins are distributed along the cytoskeleton in a spiral-like structure (31-34), and the secretion of Colibactin-maturating enzyme (CIbp) across the IM is MreB and Sec/SRP/YidC dependent (35). To reflect this body of literature, we extended our hypothesis to propose that MreB

bioRxiv preprint doi: https://doi.org/10.1101/305441; this version posted April 24, 2018. The copyright holder for this preprint (which was not certified by peer review) is the author/funder, who has granted bioRxiv a license to display the preprint in perpetuity. It is made available under aCC-BY-NC-ND 4.0 International license.

helical filaments in combination with the Sec machinery may act as a pathway to deliver ATs toward bacterial poles.

To investigate the localization patterns of autotransporters as they are secreted from a bacterial cell we used two separate methods of fluorescent labelling to follow ATs with proteolytic passenger domains (EspC and AaaA) as they move out of the bacterial cell. We show for the first time that AT localization is dependent on a dynamic interaction with a cellular structure reliant upon the actin homologue MreB, and the Sec translocon, and occurs in a helical distribution along the bacterial cytoskeleton.

Results

ATs with protease activity localize to a spiral structure resembling the bacterial cytoskeleton. To track localization during secretion, two fluorescent tags were introduced into two protease ATs. A cell-tethered AT (AaaA) and an extracellularly released AT (EspC) were selected to identify common secretion pathways. Fusion of the ATs to the monomeric variant of DsRed fluorescent protein, mCherry, provided fluorescence directly (36,37). The other tag (i) involved fusion to a smaller polypeptide, the tetracysteine (TC) motif (two cysteine pairs flanking Proline and Glycine residues), and (ii) provided enhanced experimental control in the timing of labelling since it requires exogenous addition of the biarsenical labelling reagent FlAsH-EDT_2 to become fluorescent (38). The mCherry was fused adjacent to Lys residue 340 of the EspC passenger domain (Fig. S1*A*). We predicted this site would not disrupt the EspC catalytic serine at position 256 (39). The TC-motif was genetically engineered into the EspC passenger domain between Gln530 and Phe531. The *in situ* modelled structure of EspC predicts this site is externally exposed, and distant from the active sites, and would thus be easily accessible by the FlAsH substrate without affecting the function of the target protein (Fig. S1*B*).

Fluorescence microscopy revealed that EspC-mCherry was distributed in patches. Some was at the cell poles and some distributed along the length of the cell in a defined helical arrangement (Fig. 1*A* left panel and 1*B*). Stacking individual confocal sections revealed the extended helical patterns along the length of the cell in 48% of the bacteria examined (Fig. 1*C* and Movie *S1*). Control bacteria producing native mCherry (Fig. S2) exhibited diffuse cytoplasmic localization throughout the cell as expected (right panel Fig. 1*A*). EspC labelled with FlAsH (EspC-TC) also acquired a spiral patchy localization (Fig. 2*A* and Fig. S3). No spiral fluorescence was observed with the unlabelled control EspC. Super resolution microscopy (SR-SIM) revealed that the 3D helix was formed from patches of protein encircling the cell wall of the bacterium (Fig. 2*B*). 3D rendering of structured illumination images allowed a panoramic inspection inside the bacterium during EspC

bioRxiv preprint doi: https://doi.org/10.1101/305441; this version posted April 24, 2018. The copyright holder for this preprint (which was not certified by peer review) is the author/funder, who has granted bioRxiv a license to display the preprint in perpetuity. It is made available under aCC-BY-NC-ND 4.0 International license.

secretion (Fig. 2*C* and Movie S2). The striking spiral distribution of EspC molecules was evident at the boundary of the membranes or within the periplasm. Patches of fluorescence were clearly apparent around the cell membranes, stretching along the bacterial cytoskeleton from pole to pole (Fig. 2*C* and Movie S2). Most notably the lack of the FlAsH labelled EspC within the bacterial cytoplasm highlighted the distinct possibility that the bacterial cytoskeleton could be driving some kind of localization during AT secretion.

To test whether the observed localization represents a common underlying secretion pathway for ATs, localization of the surface exposed AT AaaA was compared with that of EspC. The TC sequence was inserted after the Leucine residue at codon 291 of AaaA to optimise fluorescence whilst minimising disruption of AT activity creating AaaA-TC (Fig. S4). Confocal fluorescence microscopy revealed that FlAsH-labelled AaaA-TC was localized in patches orientating circumferentially around and along the long axis of the cell (Fig.3*A*). Z-stack confocal images further supported the AaaA localization as a helical array (Fig.3*B*). Control bacteria producing the AaaA that was not labelled by the FIAsH substrate showed very weak diffuse fluorescence signals (Fig.3*A*). Higher resolution SR-SIM confirmed that during secretion AaaA localized to patchy helices around the bacterial circumference very similar to those of EspC (Fig.3*C* and Movie S3).

Spiral formation was dependent upon the presence of the AT β-barrel. A truncated version of EspC-mCherry lacking the C-terminal β-barrel domain (produced from plasmid p33tespCmcherry, Fig. S5) exhibited a diffuse localization with polar accumulation that lacked a helical structure in 100% of the bacteria examined (Central panel, Fig. 1*A*). Likewise, truncated AaaA-TC lacking the C-terminal β-barrel domain (AaaA-TCΔ) did not localize to a helix (Fig. 3*A* right panel). AaaA-TCΔ was engineered by introduction of an amber stop codon (TAG) at amino acid position 343 in the sequence of AaaA-TC (which is equivalent to position 338 in the native AaaA sequence). Unlike truncated EspC-mCherry, AaaA-TCΔ localized to dense foci (blobs) distributed along the long axis of the cells (Fig. 3*A* right panel). Optical sections of a bacterium producing FlAsH labelled AaaA-TCΔ confirmed the absence of the spiral localization array (Fig. 3*C*, Movie S4 and Fig. S6).

Perturbing the actin homologue MreB alters the helical organization of ATs. To test the possibility that the bacterial cytoskeleton actin homologue MreB influences the spiral arrangement of EspC and AaaA during secretion, the localization of MreB was first tracked. To visualize the localization pattern of MreB, the TC motif was inserted by engineering *mreB* to encode two cysteine residues before and after residues Pro227–Gly228 using site-directed mutagenesis (Fig. S7). As shown in the Fig. 4 *A* and *B*, FlAsH labelling of MG1655 producing MreB-TC showed that MreB is localized in patchy patterns.

bioRxiv preprint doi: https://doi.org/10.1101/305441; this version posted April 24, 2018. The copyright holder for this preprint (which was not certified by peer review) is the author/funder, who has granted bioRxiv a license to display the preprint in perpetuity. It is made available under aCC-BY-NC-ND 4.0 International license.

In most bacteria (62% of those examined), these patches spanned the entire length of the cell. Consistent with previous reports (40), in some bacteria (35% of those examined), short filaments diagonally followed the curve of the cells. The patchy structural pattern of MreB was particularly evident using advanced super resolution, dSTORM analysis (Fig. 4*C*).

Next, to verify the contribution of MreB to AT localization, we inhibited MreB filament assembly using the compound A22. It has been reported that the effect of A22 is similar to the effect of a MreB null mutant (41). In order to monitor EspC-mCherry localization patterns in the presence of A22, arabinose induced MG1655(p33espCmcherry) hosting the full length EspC-mCherry and MG1655(p33tespCmcherry) containing the truncated EspC-mCherry version were treated with $A22^{10}$. As a control, a set of samples were induced and grown without treatment ($A22^{0}$). As a consequence of using the MreB filament inhibitor A22, the morphology of the bacterial cells was changed from rod to rounded shapes as expected (Fig. 5*A*). The fluorescent localization patterns of both full length and truncated EspC-mCherry forms dramatically changed. Following treatment with $A22^{10}$, the fluorescent localization pattern of full length EspC-mCherry was completely disrupted and appeared diffuse with no distinct spiral arrangement. In contrast, the truncated version of EspC-mCherry lacking the β-barrel was observed as strong diffuse fluorescence with irregular punctate foci (Fig. 5*B*).

Inactivation of SecA alters the localization of ATs. Sec has been reported to be maintained in a spiral localization (33). To investigate the intracellular localization of EspC in the absence of Sec, p33espCmcherry, p33tespCmcherry and pmLA33Cherry (control) were transformed into a SecA mutant of *E. coli* (MM52) and fluorescence microscopy was undertaken. Interestingly, both forms of EspC-mCherry exhibited localization patterns different to those observed previously. In *E. coli*ΔsecA grown at the non-permissive temperature, full length EspC-mCherry produced a bipolar and mildly diffuse localization whereas truncated EspC-mCherry was diffusely distributed or unipolar (Fig. 5*C*). Notably, the control *E. coli*Δ*secA*(pmLA33Cherry) exhibited the same diffuse patterns of fluorescence as observed before (Fig. 5*C*). The bipolar distribution of ATs in the absence of SecA was even more pronounced when the localization of AaaA was tracked in *E. coli*Δ*secA*(p33aaaA-TC) stained with FlAsH (Fig. 5*D*).

The EspC spiral formation is unlikely to be an artefact of aggregation. Labelling EspC with the large 30 kDa mCherry fluorescent protein may interfere with its journey toward the bacterial surface and cause protein misfolding or premature folding (aggregates) resulting in fluorescence artefacts (42). To discount this, whole cell extracts

bioRxiv preprint doi: https://doi.org/10.1101/305441; this version posted April 24, 2018. The copyright holder for this preprint (which was not certified by peer review) is the author/funder, who has granted bioRxiv a license to display the preprint in perpetuity. It is made available under aCC-BY-NC-ND 4.0 International license.

induced by 0.02% arabinose from MG1655(p33espCmcherry) and the control MG1655(pBAD33) strains were subjected to floatation sucrose gradient fractionation and immunoblotting (see *Material and Methods*). This method was selected because it provides a good separation of membrane associated proteins from aggregated proteins (43). Importantly, the full length EspC-mCherry protein was mostly located in the fraction containing 55% sucrose which was the same fractions shown for the folded OM protein, TolC. There was also no detection of any EspC at higher sucrose concentrations (58-61%) which are associated more with aggregated proteins suggesting that the full length EspC-mCherry is associated with the OM in a folded state (Fig. 6*A*). No EspC was detected in total cell extracts from the control MG1655(pBAD33) strain (Fig. S8*A*). To further explore if different expression levels of EspC-mCherry might cause localization artefacts as a consequence of formation of aggregates, the floatation gradient analysis was repeated using whole cell extracts from MG1655(p33espCmcherry) induced with the higher (0.2%) and lower doses (0.002%) of arabinose. Similar results were obtained (Fig. S8*B),* which indicate that the EspC helix forms at different protein production levels, discounting the possibility of it being an artefact.

To verify that the formation of helically localized ATs was not an artefact arising from high protein production levels (37), we sought to reduce the protein production to the lowest detectable level. The microscopy data shown so far in this study was obtained using AT induction with 0.02% arabinose. Fig. 6*B* shows that culture of MG1655(p33espCmcherry) induced for 4 h with 0.002% arabinose was more than enough to observe the discrete patches and spiral patterns of EspC-mCherry inside bacteria.

The helical localization of AT along the cytoskeleton is dynamic and transient. The circumferentially distributed disconnected patches of both EspC and AaaA hint at a dynamic spiral path being followed by the ATs during secretion. To assess the potential dynamic nature of these patches, fluorescence recovery after photobleaching (FRAP) was used in live cells producing full length EspC-mCherry fusion to determine if the localization of molecules is transient. As a control, AaaA-TC was also exploited in this experiment due to the different fluorescent labelling technique that requires addition of a substrate (FlAsH-EDT_2) to produce fluorescence. MG1655(p33espCmcherry) was grown, induced with 0.02% arabinose for 4 h and prepared for confocal imaging as previously described. As shown in Fig. 7*A*, a selected single fluorescent patch (green circle) located close to the middle of the bacterium was photobleached using a focused laser beam and the recovery of fluorescence was monitored for up to 35 min. Interestingly, the EspC-mCherry patch showed a good recovery of fluorescence over time (Fig. 7*C*). The Zeiss FRAP analysis

bioRxiv preprint doi: https://doi.org/10.1101/305441; this version posted April 24, 2018. The copyright holder for this preprint (which was not certified by peer review) is the author/funder, who has granted bioRxiv a license to display the preprint in perpetuity. It is made available under aCC-BY-NC-ND 4.0 International license.

revealed that the percentage of mobile and static foci was 67.93% and 32.07% respectively inside the green circle.

However, as expected, bleaching one discrete patch of fluorescent AaaA-TC on the cell did not show any fluorescence recovery over time (Fig. 7*B* and *D*). Here, the percentage of mobile and static foci was 0.4% and 99.6% respectively inside the green circle. These results support the notion that the EspC-mCherry molecules are mobile, and when newly synthesized they are able to enter pathways of secretion that are visualized as fluorescent patches in this study.

Discussion

Our data show that the cytoskeleton created by the bacterial actin homologue, MreB, could act with the Sec translocon as a scaffold to provide a pathway for membrane protein localization and diffusion. Our findings demonstrate this pathway is utilized by pivotal bacterial virulence factors (the ATs). It is a relatively recent notion that bacteria have a sophisticated spatial organization. Consequently, the underlying mechanisms integral to the formation and function of bacterial subcellular compartmentalisation remain to be elucidated in full. It is clear that the components impact upon many fundamental cellular process including ones with parallels across eukaryotes and prokaryotes such as the general secretion system and the cytoskeleton. The ability of MreB, like actin, to assemble and disassemble from filaments could provide a hitherto elusive propulsive force that enables ATs to traverse from the IM to the OM for secretion in the absence of ATP (10), and is substantiated by our observation that the interaction is dynamic and transient. MreB filaments assemble with MreC, MreD, PBP2 and RodA. This assembly is dependent on the presence of the FtsZ ring component of the cell division apparatus (23,44), and the treadmilling motion generated by FtsZ could add a source of propulsive energy. In *E. coli*, MreB filaments are connected directly with the IM through an interaction between the MreB N-terminal amphipathic helix and the cytoplasmic part of the RodZ ring creating antiparallel double helical filaments (44,45). There is also now evidence that links with the Sec translocon providing a mechanism to integrate organization on both sides of the IM (30), and a potential route for the ATs to dock with BAM or TAM in the OM. One potential mechanism could be targeting of the Sec translocon by the AT towards the mid-point of the cell followed by propulsion towards the poles by a mechanism driven by MreB providing time to collide with the BAM and/or TAM and subsequent translocation across the OM and final secretion close to the poles (Fig. S9).

Originally proposed as autonomous proteins using the simplest secretion machinery, it is emerging that autotransporters rely on numerous components of the cell

bioRxiv preprint doi: https://doi.org/10.1101/305441; this version posted April 24, 2018. The copyright holder for this preprint (which was not certified by peer review) is the author/funder, who has granted bioRxiv a license to display the preprint in perpetuity. It is made available under aCC-BY-NC-ND 4.0 International license.

envelope for their assembly. Understanding this mechanism at a molecular level provides the potential to understand fundamental pathways central to the physiology of bacteria with which the ATs interact during their secretion, for example SecA and MreB, and offers the potential to identify novel antimicrobials targeted towards virulence factors. Interestingly, the Gram-positive cell division protein DivIVA (46) also interacts with SecA, but it is not known if this occurs directly or indirectly *in vivo*, nor what the nature of co-dependence is. An important next step is to demonstrate these protein interactions directly. For the AT EspC, there is also the intriguing mystery of how it might interact with the type 3 secretion machinery (T3SS) for delivery to eukaryotic cells without being secreted through the T3SS (47,48). Could this be mediated via a co-dependence on MreB?

It was striking how the ATs were so distinctly located in the cell envelope. The use of fluorescent tags such as fluorescent proteins and fluorescently labelled antibodies in protein localization studies has had a huge impact on discovering and understanding the molecular basis of various molecules in both eukaryotic and prokaryotic cells (37). However, the use of large fluorescent tags bears the risk of causing localization artefacts since they may interfere with the protein's function, and must be carefully controlled (37). Swulius and Jensen, 2012 used cryotomographic microscopy to illustrate that the spiral filament formation by MreB fused with yellow fluorescent protein (YFP) at its N-terminus is an artefact, whereas when MreB was tagged within an internal loop with mCherry, it showed a patchy localization pattern similar to that of native MreB (49). Utilization of monomeric rather than dimeric YFP also avoided any unnecessary inaccuracies in the interpretation of aggregation patterns of MreB (37). In this study, fusion of two ATs to mCherry or utilization of the much smaller TC motif and FlAsH substrate generated similar localization patterns and provided the added benefit of revealing the dynamic nature of the interaction between the AT and the bacterial cytoskeleton.

Materials and Methods

Bacterial strains, Plasmids and Growth culture

The bacterial strains used in this study (Table S1) were routinely grown on Luria-Bertani (LB) agar or liquid shaking at 37°C with chloramphenicol (25 µg/ml), ampicillin (100 µg/ml) or Streptomycin (100 µg/ml) when appropriate and kept frozen at -80°C in 25% (v/v) glycerol for future use. Bacterial growth was monitored by estimating optical densities at 600 nm using a 1 in 10 dilution of cultures into the growth medium to ensure accurate spectrophotometer readings. *E. coli* ΔSecA strains were grown at 30°C up to 0.5 OD_{600} then switched to non-permissive temperature at 42°C. To express the recombinant protein, bacterial overnight cultures were diluted 1:100 and induced concurrently with

bioRxiv preprint doi: https://doi.org/10.1101/305441; this version posted April 24, 2018. The copyright holder for this preprint (which was not certified by peer review) is the author/funder, who has granted bioRxiv a license to display the preprint in perpetuity. It is made available under aCC-BY-NC-ND 4.0 International license.

0.2% or 0.02% (w/v) L-arabinose (final concentration from Sigma) as required for up to 4 h shaking at 37°C unless otherwise stated. All plasmids used in this study are listed in supplementary Table S2 and were introduced into freshly prepared $CaCl_2$ competent cells by heat shock at 42°C for 4 min.

DNA manipulation and cloning

Oligonucleotide primers (Table S3) were designed using American SnapGene® software and were manufactured by Sigma. Plasmid DNA was purified using a plasmid purification kit (Qiagen) or GenElute™ Plasmid Miniprep Kit (Sigma). Restriction enzyme digestion, ligation and agarose gel electrophoresis were performed using standard methods (50). Routinely PCR reactions were performed using the Q5® High-Fidelity 2X Master Mix kit (NEB) following the manufacturer's instructions. DNA products were agarose gel electrophoresis in 1X tris-acetate-ethylenediaminetetraacetic acid (TAE) buffer (40 mM Tris base pH 7.8, 50 mM EDTA and 0.1142% Glacial acetic acid) for 60 min at 100 volt and for size estimation, Tri Dye™ 1kb DNA ladder (NEB) was used in parallel to the samples during separation after adding Blue/Orange Loading Dye, 6X (Promega). Extraction of the DNA from agarose gel was performed by using Gel extraction kit (Qiagen), whereas for DNA purification a PCR purification kit (Qiagen) was used. When necessary, DNA sequencing was conducted by Source BioScience, Nottingham, using Sanger sequencing services and ABI3730XL sequencer. Alignment of DNA or protein sequences to identify homology was achieved using the Basic Local Alignment Search Tool 'BLAST' provided by NCBI (http://blast.ncbi.nlm.nih.gov/Blast.cgi). The Sequences of the pre- determined DNA and protein were obtained from the NCBI (http://www.ncbi.nlm.nih.gov/) using gene and protein databases respectively. The plasmids used or generated in this study are listed in Table S2, the primers used in Table S3, and the cloning schemes shown in Fig. S1, S2, S4, S5, S7. The gene encoding mCherry was cloned into pBAD33 to create p33mcherry by amplifying the mCherry encoding gene from pmCherry (cite Shaner et al 2004) using F-BglII mCherry/R-SalI mCherry primers designed to introduce BglII and SalI sites at the 5' and 3' ends of the mCherry coding region respectively. Levels and activities of the recombinant ATs are shown in Fig. S10-S11.

Transformation

Transformation of *E. coli* was carried out using chemical transformation. Competent cells were prepared using 100 mM $CaCl_2$, (ice cold). Heat shock was performed by first adding 100 ng of DNA to 300 µl of fresh prepared $CaCl_2$ competent cells followed by 45 min on ice, 4 min at 42°C and 4 min on ice then 500µl of fresh LB added followed by incubation

bioRxiv preprint doi: https://doi.org/10.1101/305441; this version posted April 24, 2018. The copyright holder for this preprint (which was not certified by peer review) is the author/funder, who has granted bioRxiv a license to display the preprint in perpetuity. It is made available under aCC-BY-NC-ND 4.0 International license.

at 37°C (shaking) for 60 min. Subsequently, after finishing the incubation period, centrifugation for 2 min at 5000 rpm following by resuspending the pellet in 200 µl of fresh LB, spreading them on selectable antibiotic plates as appropriate, and incubating overnight at 37°C. To confirm the cloning of the desired gene with or without mutation, sequencing was accomplished by DNA sequencing service analysis facility unit in Source Bioscience Life Sciences Company based in Nottingham.

Site directed mutagenesis

Site-directed mutagenesis was carried out by following the principles described in the QuikChange II Site-Directed Mutagenesis Kit, Instruction manual (from Agilent Technology). To obtain high mutation efficiencies, the high fidelity *Pfu* DNA polymerase was used (Promega). To avoid the existence of any parental templates in the PCR products, the products were digested by *DpnI* enzyme (Promega) at 37°C for 1 h following by transformation into *E. coli* Top10 to repair the nicks. Mutated plasmids were further extracted and transformed into freshly prepared $CaCl_2$ MG1655 for further analysis. Both forward and reverse primers (Table *S*3) were designed by SnapGene software to whether insert or substitute particular nucleotides on desired fragments to generate mutations. Mutation was confirmed by fully sequencing of mutated genes using primers listed in Table *S*3.

Sodium dodecyl sulphate-polyacrylamide gel electrophoresis (SDS-PAGE) and Immunoblotting

SDS-PAGE and immunoblotting were performed as described previously (50) using 9% SDS-PAGE gels. To enable detection of EspC, AaaA, mCherry, TolC and AcrB proteins, the rabbit α-EspC was used at concentration 1:1000, rabbit α-AaaA was used at 1:1000, rabbit α-TolC used at 1:2000 and rabbit α-AcrB used at 1:2000 respectively as primary antibodies, whereas the goat anti-rabbit IgG conjugated to horseradish peroxidase (HRP) (Sigma) was used at a dilution of 1:10,000 as secondary antibody. All antibodies were incubated for 1h at room temperature shaking and washed with PBST 0.5%.

bioRxiv preprint doi: https://doi.org/10.1101/305441; this version posted April 24, 2018. The copyright holder for this preprint (which was not certified by peer review) is the author/funder, who has granted bioRxiv a license to display the preprint in perpetuity. It is made available under aCC-BY-NC-ND 4.0 International license.

The S-(3.4-Dichlorobenzyl)-isothiourea (A22)

To perturb the bacterial actin homologue cytoskeleton MreB, A22 (Calbiochem) was used in this study according to the previous study made by Gitai *et al*., 2005 (41). A22 was prepared at concentration 5 mM (stock concentration) and used either at zero µg/ml ($A22^0$) as untreated controls or 10 µg/ml ($A22^{10}$) to have completely circular cells. Bacterial strains to be tested were grown in LB broth plus appropriate antibiotics O/N at 37°C shaking 200 rpm. Next day, 1 ml of cultures was used to inoculate 99 ml of fresh LB broth supplemented with antibiotics (1:100 dilution) using 500 ml flask and concurrently induced by 0.2% arabinose. The cultures kept to grow shaking at 37°C for approximately 1 h (until reach 0.05 of OD_{600nm}). At this particular point, the cultures were aliquoted into 2 sets (25 ml each in 100 ml flasks). One set of culture was treated with $A22^0$ (control) and the second set was with $A22^{10}$. Subsequently, treated cells were incubated to grow at 37°C shaking for further 4 h, harvested by centrifugation at 6000 rpm for 5 min, washed once with ice cold PBS, and resuspended to 0.5 OD_{600} units/ml. Finally, 8 µl of washed cells were applied on microscopic slides for microscope analysis.

Subcellular fractionation and sucrose gradient analysis

The sucrose gradients fractionation was undertaken as described previously (43).

FlAsH labelling of tetracysteine-tagged recombinant proteins

To enable detection of recombinant proteins hosting tetracysteine motif, the green membrane-permeable biarsenical dye, FlAsH-EDT_2 (Invitrogen), was used in this study. Cultures of the strains to be tested were prepared and induced by 0.02% arabinose as previously described unless otherwise stated. Cells producing TC-tagged protein were harvested by centrifugation at 5500 rpm for 2 min and washed once with 1x HEPES buffered saline BioUltra (Sigma), ice cold, and resuspended in 1 ml to 1.0 of OD_{600} using the same buffer. The cells were centrifuged once more and the pellet was resuspended (slowly) in 500 µl 1x HEPES buffer containing 3-5 µM (final concentration) FlAsH-EDT_2 substrate followed by incubation for 35-45 min in darkness at RT. After incubation, cells were harvested by centrifuging as before and the supernatant discarded according to the University of Nottingham guidelines. Subsequently, cells were washed twice with 1 ml 1x British Anti-Lewisite (BAL) wash buffer at final concertation of 0.25 mM as recommended by the manufacturer (added twice volume of wash buffer to the volume of added substrate). Lastly, cells were further washed once again with the 1x HEPES buffered saline, ice cold and resuspended to approximately 0.5 of OD_{600}. 8 µl of washed cells were mounted

bioRxiv preprint doi: https://doi.org/10.1101/305441; this version posted April 24, 2018. The copyright holder for this preprint (which was not certified by peer review) is the author/funder, who has granted bioRxiv a license to display the preprint in perpetuity. It is made available under aCC-BY-NC-ND 4.0 International license.

on microscope slide, covered with coverslip, sealed with transparent nail polish and examined by fluorescence microscope.

Confocal fluorescence microscope

To generate more detailed images, a Zeiss LSM 700 confocal laser scanning microscope was used fitted with HXP 120C lamp for light illumination and a Zeiss alpha-Plan-Apochromat 63x/1.46 Oil objective lens. Images were captured by using AxioCam digital microscopecamera connected to ZEN software and analysed using image J software. Occasionally, in order to facilitate visualising the EspC-mCherry fluorescent patterns, cultures were sampled, stained with the lipophilic fluorescent membrane stain, FM 1-43 (Invitrogen) according to the manufacturer's instructions. Briefly, cell pellets were resuspended in 1 ml ice cold PBS containing 5 µg/ml FM-1 43 (final concentration) and incubated on ice for a maximum 1 min in darkness and washed twice with ice cold PBS before mounting on microscope sides.

Fluorescence recovery after photobleaching (FRAP) experiment

The microscope Zeiss Elyra PS.1, with alpha-Plan-Apochromat 100x/1.46 Oil DIC M27 Elyra objective in confocal mode was used for FRAP experiment. Images acquired using 561 nm laser at 2.0% or 488 laser at 0.3% for mCherry and FlAsH-tag respectively. Zeiss Zen Black 2012 software was used to extract the intensity values from the bleached and control regions over time. Drift correction was applied using Zen Blue 2012 software. Values were exported to Microsoft Excel and normalization was done by dividing the values from the bleached zone with the values from the control zone before values were plotted.

Super resolution microscope

For super-resolution imaging a Zeiss Elyra PS.1 microscope was used in SIM (structured illumination microscopy) or dSTORM (direct stochastic optical reconstruction microcopy) modes. In SIM mode, either Plan-Apochromat 63x/1.4 Oil DIC M27 or C-Apochromat 63x/1.2W Korr M27 objectives were used. For FlAsH labelled bacteria the following setting were used in SIM mode; filter set LBF-488/561, laser power 488 nm at 4.0% and cmos camera exposure time 25.0 ms. On the other hand, BP 570-620+LP 750 filter, 561 nm laser at 2.1% and camera exposure 100.0 ms were used for mCherry expressing bacteria. With regarding to the dSTORM mode, the following setting was utilized; alpha Plan-Apochromat 100x/1.46 Oil DIC M27 Elyra objective, BP 495-550+LP 750 filter 488 nm laser at 100% and 405 nm laser at 1% (this is used to increase the number of molecules which return to ground state, and therefore more molecules will emit light), 100 ms exposure, EM-CCD gain 200.

bioRxiv preprint doi: https://doi.org/10.1101/305441; this version posted April 24, 2018. The copyright holder for this preprint (which was not certified by peer review) is the author/funder, who has granted bioRxiv a license to display the preprint in perpetuity. It is made available under aCC-BY-NC-ND 4.0 International license.

Acknowledgements

We would like to thank Libyan Embassy (Cultural Attaché – London) and the School of Life Sciences postgraduate support team for financially supporting MA and Biotechnology and Biological Sciences Research Council UK for providing the means to establish Superresolution Microscopy infrastructure with which to deliver the analysis (BBSRC BB/L013827/1). We also thank colleagues at the University of Nottingham Centre for Biological Sciences for supporting this study, in particular Louise Arnold and Stephanie Pommier for making plasmids p33espC and p33espCmcherry respectively, and to Mathulah Sriskandarajah for performing some of the AaaA activity assays.

Author contributions

Mahmoud Ashawesh generated all the data in this study working closely with Robert Markus to produce and analyse high quality images on the super resolution microscope. Kim Hardie conceived, directed and wrote the manuscript with input from Mahmoud Ashawesh and Christopher Penfold.

References

1. Huttner, A., Harbarth, S., Carlet, J., Cosgrove, S., Goossens, H., Holmes, A., Jarlier, V., Voss, A., and Pittet, D. (2013) Antimicrobial resistance: a global view from the 2013 World Healthcare-Associated Infections Forum. *Antimicrobial resistance and infection control* **2**, 31
2. WHO. (2014) *Antimicrobial resistance: global report on surveillance*
3. Casadevall, A., and Pirofski, L. (2001) Host-pathogen interactions: the attributes of virulence. *The Journal of infectious diseases* **184**, 337-344
4. Stephens, C., and Shapiro, L. (1997) Bacterial protein secretion--a target for new antibiotics? *Chemistry & biology* **4**, 637-641
5. Rao, C. V. S., De Waelheyns, E., Economou, A., and Anne, J. (2014) Antibiotic targeting of the bacterial secretory pathway. *Biochimica et biophysica acta* **1843**, 1762-1783
6. Baron, C., and Coombes, B. (2007) Targeting bacterial secretion systems: benefits of disarmament in the microcosm. *Infectious disorders drug targets* **7**, 19-27
7. Costa, T. R., Felisberto-Rodrigues, C., Meir, A., Prevost, M. S., Redzej, A., Trokter, M., and Waksman, G. (2015) Secretion systems in Gram-negative bacteria: structural and mechanistic insights. *Nature reviews. Microbiology* **13**, 343-359
8. Baron, C. (2013) A novel strategy to target bacterial virulence. *Future microbiology* **8**, 1-3

bioRxiv preprint doi: https://doi.org/10.1101/305441; this version posted April 24, 2018. The copyright holder for this preprint (which was not certified by peer review) is the author/funder, who has granted bioRxiv a license to display the preprint in perpetuity. It is made available under aCC-BY-NC-ND 4.0 International license.

9. van Ulsen, P., Rahman, S., Jong, W. S., Daleke-Schermerhorn, M. H., and Luirink, J. (2014) Type V secretion: from biogenesis to biotechnology. *Biochimica et biophysica acta* **1843**, 1592-1611

10. Albenne, C., and Ieva, R. (2017) Job contenders: roles of the beta-barrel assembly machinery and the translocation and assembly module in autotransporter secretion. *Molecular microbiology* **106**, 505-517

11. Rossiter, A. E., Leyton, D. L., Tveen-Jensen, K., Browning, D. F., Sevastsyanovich, Y., Knowles, T. J., Nichols, K. B., Cunningham, A. F., Overduin, M., Schembri, M. A., and Henderson, I. R. (2011) The essential beta-barrel assembly machinery complex components BamD and BamA are required for autotransporter biogenesis. *Journal of bacteriology* **193**, 4250-4253

12. Webb, C. T., Heinz, E., and Lithgow, T. (2012) Evolution of the beta-barrel assembly machinery. *Trends in microbiology* **20**, 612-620

13. Henderson, I. R., Navarro-Garcia, F., Desvaux, M., Fernandez, R. C., and Ala'Aldeen, D. (2004) Type V protein secretion pathway: the autotransporter story. *Microbiology and molecular biology reviews : MMBR* **68**, 692-744

14. Kjaergaard, K., Schembri, M. A., Hasman, H., and Klemm, P. (2000) Antigen 43 from Escherichia coli induces inter- and intraspecies cell aggregation and changes in colony morphology of Pseudomonas fluorescens. *Journal of bacteriology* **182**, 4789-4796

15. Reyrat, J. M., Charrel, M., Pagliaccia, C., Burroni, D., Lupetti, P., de Bernard, M., Ji, X., Norais, N., Papini, E., Dallai, R., Rappuoli, R., and Telford, J. L. (1998) Characterisation of a monoclonal antibody and its use to purify the cytotoxin of Helicobacter pylori. *FEMS microbiology letters* **165**, 79-84

16. Wilhelm, S., Tommassen, J., and Jaeger, K. E. (1999) A novel lipolytic enzyme located in the outer membrane of Pseudomonas aeruginosa. *Journal of bacteriology* **181**, 6977-6986

17. Luckett, J. C., Darch, O., Watters, C., Abuoun, M., Wright, V., Paredes-Osses, E., Ward, J., Goto, H., Heeb, S., Pommier, S., Rumbaugh, K. P., Camara, M., and Hardie, K. R. (2012) A novel virulence strategy for Pseudomonas aeruginosa mediated by an autotransporter with arginine-specific aminopeptidase activity. *PLoS pathogens* **8**, e1002854

18. Stein, M., Kenny, B., Stein, M. A., and Finlay, B. B. (1996) Characterization of EspC, a 110-kilodalton protein secreted by enteropathogenic Escherichia coli which is homologous to members of the immunoglobulin A protease-like family of secreted proteins. *Journal of bacteriology* **178**, 6546-6554

19. Ruiz-Perez, F., and Nataro, J. P. (2014) Bacterial serine proteases secreted by the autotransporter pathway: classification, specificity, and role in virulence. *Cellular and molecular life sciences : CMLS* **71**, 745-770

20. Jain, S., van Ulsen, P., Benz, I., Schmidt, M. A., Fernandez, R., Tommassen, J., and Goldberg, M. B. (2006) Polar localization of the autotransporter family of large bacterial virulence proteins. *Journal of bacteriology* **188**, 4841-4850

21. Janakiraman, A., Fixen, K. R., Gray, A. N., Niki, H., and Goldberg, M. B. (2009) A genome-scale proteomic screen identifies a role for DnaK in chaperoning of polar autotransporters in Shigella. *Journal of bacteriology* **191**, 6300-6311

22. Fixen, K. R., Janakiraman, A., Garrity, S., Slade, D. J., Gray, A. N., Karahan, N., Hochschild, A., and Goldberg, M. B. (2012) Genetic reporter system for positioning of proteins at the bacterial pole. *mBio* **3**

23. Vats, P., Shih, Y. L., and Rothfield, L. (2009) Assembly of the MreB-associated cytoskeletal ring of Escherichia coli. *Molecular microbiology* **72**, 170-182

bioRxiv preprint doi: https://doi.org/10.1101/305441; this version posted April 24, 2018. The copyright holder for this preprint (which was not certified by peer review) is the author/funder, who has granted bioRxiv a license to display the preprint in perpetuity. It is made available under aCC-BY-NC-ND 4.0 International license.

24. van Teeffelen, S., and Gitai, Z. (2011) Rotate into shape: MreB and bacterial morphogenesis. *The EMBO journal* **30**, 4856-4857

25. Strahl, H., Burmann, F., and Hamoen, L. W. (2014) The actin homologue MreB organizes the bacterial cell membrane. *Nature communications* **5**, 3442

26. Gitai, Z., Dye, N., and Shapiro, L. (2004) An actin-like gene can determine cell polarity in bacteria. *Proceedings of the National Academy of Sciences of the United States of America* **101**, 8643-8648

27. van Teeffelen, S., Wang, S., Furchtgott, L., Huang, K. C., Wingreen, N. S., Shaevitz, J. W., and Gitai, Z. (2011) The bacterial actin MreB rotates, and rotation depends on cell-wall assembly. *Proceedings of the National Academy of Sciences of the United States of America* **108**, 15822-15827

28. Cowles, K. N., and Gitai, Z. (2010) Surface association and the MreB cytoskeleton regulate pilus production, localization and function in Pseudomonas aeruginosa. *Molecular microbiology* **76**, 1411-1426

29. Shih, Y. L., Kawagishi, I., and Rothfield, L. (2005) The MreB and Min cytoskeletal-like systems play independent roles in prokaryotic polar differentiation. *Molecular microbiology* **58**, 917-928

30. Govindarajan, S., and Amster-Choder, O. (2017) The bacterial Sec system is required for the organization and function of the MreB cytoskeleton. *PLoS genetics* **13**, e1007017

31. Matsumoto, K., Hara, H., Fishov, I., Mileykovskaya, E., and Norris, V. (2015) The membrane: transertion as an organizing principle in membrane heterogeneity. *Frontiers in microbiology* **6**, 572

32. Shiomi, D., Yoshimoto, M., Homma, M., and Kawagishi, I. (2006) Helical distribution of the bacterial chemoreceptor via colocalization with the Sec protein translocation machinery. *Molecular microbiology* **60**, 894-906

33. Campo, N., Tjalsma, H., Buist, G., Stepniak, D., Meijer, M., Veenhuis, M., Westermann, M., Muller, J. P., Bron, S., Kok, J., Kuipers, O. P., and Jongbloed, J. D. (2004) Subcellular sites for bacterial protein export. *Molecular microbiology* **53**, 1583-1599

34. Gold, V. A., Robson, A., Bao, H., Romantsov, T., Duong, F., and Collinson, I. (2010) The action of cardiolipin on the bacterial translocon. *Proceedings of the National Academy of Sciences of the United States of America* **107**, 10044-10049

35. Cougnoux, A., Gibold, L., Robin, F., Dubois, D., Pradel, N., Darfeuille-Michaud, A., Dalmasso, G., Delmas, J., and Bonnet, R. (2012) Analysis of structure-function relationships in the colibactin-maturating enzyme ClbP. *Journal of molecular biology* **424**, 203-214

36. Shaner, N. C., Campbell, R. E., Steinbach, P. A., Giepmans, B. N., Palmer, A. E., and Tsien, R. Y. (2004) Improved monomeric red, orange and yellow fluorescent proteins derived from Discosoma sp. red fluorescent protein. *Nature biotechnology* **22**, 1567-1572

37. Margolin, W. (2012) The price of tags in protein localization studies. *Journal of bacteriology* **194**, 6369-6371

38. Griffin, B. A., Adams, S. R., and Tsien, R. Y. (1998) Specific covalent labeling of recombinant protein molecules inside live cells. *Science (New York, N.Y.)* **281**, 269-272

39. Navarro-Garcia, F., Canizalez-Roman, A., Sui, B. Q., Nataro, J. P., and Azamar, Y. (2004) The serine protease motif of EspC from enteropathogenic Escherichia coli produces epithelial damage by a mechanism different from that of Pet toxin from enteroaggregative E. coli. *Infection and immunity* **72**, 3609-3621

bioRxiv preprint doi: https://doi.org/10.1101/305441; this version posted April 24, 2018. The copyright holder for this preprint (which was not certified by peer review) is the author/funder, who has granted bioRxiv a license to display the preprint in perpetuity. It is made available under aCC-BY-NC-ND 4.0 International license.

40. Errington, J. (2015) Bacterial morphogenesis and the enigmatic MreB helix. *Nature reviews. Microbiology* **13**, 241-248

41. Gitai, Z., Dye, N. A., Reisenauer, A., Wachi, M., and Shapiro, L. (2005) MreB actin-mediated segregation of a specific region of a bacterial chromosome. *Cell* **120**, 329-341

42. Shemiakina, II, Ermakova, G. V., Cranfill, P. J., Baird, M. A., Evans, R. A., Souslova, E. A., Staroverov, D. B., Gorokhovatsky, A. Y., Putintseva, E. V., Gorodnicheva, T. V., Chepurnykh, T. V., Strukova, L., Lukyanov, S., Zaraisky, A. G., Davidson, M. W., Chudakov, D. M., and Shcherbo, D. (2012) A monomeric red fluorescent protein with low cytotoxicity. *Nature communications* **3**, 1204

43. Hardie, K. R., Lory, S., and Pugsley, A. P. (1996) Insertion of an outer membrane protein in Escherichia coli requires a chaperone-like protein. *The EMBO journal* **15**, 978-988

44. Salje, J., van den Ent, F., de Boer, P., and Lowe, J. (2011) Direct membrane binding by bacterial actin MreB. *Molecular cell* **43**, 478-487

45. Gerdes, K. (2009) RodZ, a new player in bacterial cell morphogenesis. *The EMBO journal* **28**, 171-172

46. Halbedel, S., Kawai, M., Breitling, R., and Hamoen, L. W. (2014) SecA is required for membrane targeting of the cell division protein DivIVA in vivo. *Frontiers in microbiology* **5**, 58

47. Kendall, M. M. (2017) Extra! Extracellular Effector Delivery into Host Cells via the Type 3 Secretion System. *mBio* **8**

48. Tejeda-Dominguez, F., Huerta-Cantillo, J., Chavez-Duenas, L., and Navarro-Garcia, F. (2017) A Novel Mechanism for Protein Delivery by the Type 3 Secretion System for Extracellularly Secreted Proteins. *mBio* **8**

49. Swulius, M. T., and Jensen, G. J. (2012) The helical MreB cytoskeleton in Escherichia coli MC1000/pLE7 is an artifact of the N-Terminal yellow fluorescent protein tag. *Journal of bacteriology* **194**, 6382-6386

50. Sambrook, J. F., Fritsch, E. F., and Maniatis, T. (1989) *Molecular Cloning: A Laboratory Manual*, 2nd ed., Cold Spring Harbor Laboratory Press, Cold Spring Harbor, NY.

51. Arnold, L. (2003) *Characterisation of factors involved in the secretion of EspC in Enteropathogenic E. coli. PhD thesis.* PhD, The University of Nottingham.

Figure Legends

Fig. 1. EspC locates to a spiral structure that resembles the bacterial cytoskeleton when it has the β-barrel domain attached. (*A*) Confocal images of *E. coli* MG1655(p33espCmcherry) producing the full length EspC-mCherry localising in a patchy helix (left panel), *E. coli* MG1655(p33tespCmcherry) producing truncated EspC-mCherry that does not adopt a helix localisation (central panel) or *E. coli* MG1655(pmLA33Cherry) producing diffusely localized mCherry which was not fused to EspC. (*B*) Imaging the red spiral structure of EspC-mCherry in *E. coli* DH5α(p33espCmcherry) by confocal microscope after staining the membrane with green FM 1-43 (top row) or in *E. coli* MG1655(p33espCmcherry) by SR-SIM (bottom row). (*C*) An extended helix is observed in *E. coli* MG1655 producing the full length EspC-mCherry. Individual confocal images of a Z stack through a cell with an extended spiral fluorescent pattern. The diagram presented in each image bottom right, corresponds to the position of the Z stack. Movie S1 is an animation of these images. An image with fully extended spiral structure was further

bioRxiv preprint doi: https://doi.org/10.1101/305441; this version posted April 24, 2018. The copyright holder for this preprint (which was not certified by peer review) is the author/funder, who has granted bioRxiv a license to display the preprint in perpetuity. It is made available under aCC-BY-NC-ND 4.0 International license.

processed by using ImageJ software which clearly shows the helix in grey (in the far right panel). Cells expressing the recombinant proteins were induced with 0.02% arabinose for 4 h in LB medium at 37°C. Samples were harvested and analysed by fluorescence microscopy as described in *Materials and Methods.* Scale bar represents 2 μm in (*A*, top row of *B*) and 1 μm in (bottom row of *B*, *C*).

Fig. 2. The spiral of FlAsH labelled EspC-TC aligns exclusively with the cell envelope. (*A*) MG1655 cells producing EspC-TC (left panel) or EspC (control, right panel) were grown in LB medium, induced with 0.02% arabinose for 4 h, stained with FlAsH and imaged by fluorescence microscopy as described in *Materials and Methods*. (*B*) Individual MG1655 cells producing EspC-TC were imaged by confocal microscopy (top row) and by SR-SIM (bottom row). The arrow in the middle picture in the bottom row mirrors the diagonal pattern of EspC around the bacterial cell circumference. (*C*) 3D rendering of structured illumination images reveal the patchy helical localization of FlAsH labelled EspC-TC within the cell envelope (longitudinal view). A 3D animation movie was created (Movie *S2*), and individual frames from 1-9 are shown here. Scale bar represents 1 μm.

Fig. 3: FlAsH-labelled AaaA-TC with an intact β-barrel domain adopts a helical patchy configuration. (*A*) Overnight cultures of MG1655 hosting p33aaaA-TC (producing AaaA containing the TC motif), p33aaaA$_{C233S}$ (producing control AaaA lacking the TC-motif and native consecutive cysteine residues), or p33taaaA-TC (producing AaaA with the TC motif but lacking the C-terminal β-barrel domain) were diluted 1:100 in LB containing 30 μg/ml Cm and grown until OD_{600} of 0.05. Cultures were induced by 0.02% arabinose for 2.5 h. Cells were prepared for FlAsH staining following the protocol described in *Materials and Methods*. Cells producing FlAsH stained AaaA-TC display patchy helical pattern whereas those producing truncated AaaA-TC localize as a dense random distribution of fluorescent spots with no structured helical arrangement. Negative control AaaAC233S was engineered to remove the two consecutive native cysteine residues (located at positions 232 and 233) that were able to interact with the FlAsH substrate in the absence of the TC tag, by exchanging cysteine 233 with serine by site directed mutagenesis. It was active and produced at comparable levels to AaaA. Confocal Z-stack sections of the bacteria producing TC-tagged truncated AaaA (*C*) lack the spirals observed with AaaA-TC (*B*). The diagrams of bisected circles (bottom left of each image) show where the focal plane was in the cell for each image in panels B and C. (*D*) 3D rendering of structured illumination images reveal the spiral localization of FlAsH labelled AaaA-TC within the cell envelope. A 3D animation movie was created (Movie S3), and individual frames from 1-9 are shown here. Scale bar represents 1 μm in (*A*) 2 μm in (*B*, *C*).

Fig. 4. FlAsH labelled MreB adopts a patchy helical distribution. (*A*) MG1655 cells hosting either p33mreB-TC (left panel), or p33mreB (control, right panel) were diluted 1:100 in LB containing 30 μg/ml Cm and induced with 0.02% arabinose for 2.5 h. Subsequently, cells were stained with FlAsH-EDT_2 (see *Material and Methods*) and imaged by confocal microscopy. (*B*) Individual FlAsH stained cells producing TC-tagged MreB display the patchy helical patterns of MreB with some short filaments that appear around the curve of the cell. (*C*) STORM image of FlAsH labelled MreB-TC shows the precise details of MreB localization in the bacterial cell wall (the centroids of the localized molecules in red pixels and the Gaussian rendering (visualises localization probability) of molecules in white

bioRxiv preprint doi: https://doi.org/10.1101/305441; this version posted April 24, 2018. The copyright holder for this preprint (which was not certified by peer review) is the author/funder, who has granted bioRxiv a license to display the preprint in perpetuity. It is made available under aCC-BY-NC-ND 4.0 International license.

clusters) which appears as a patchy distribution along the cell membranes (*C2*). Connecting the localized patches from pole to pole created a drawing of a spiral structure (*C3*). Scale bars indicate 1 µm in *A*, *B*.

Fig. 5. The patchy spiral localization of ATs is dependent on the bacterial cytoskeleton MreB and Sec translocon. (*A*) Inhibition of MreB filament assembly with A22 causes bacterial cell shape changes. MG1655 wild-type was grown in LB to OD_{600} of 0.05 then treated with $A22^0$ or $A22^{10}$ and incubated at 37°C shaking for up to 4 h as described in *Materials and Methods*. Representative rounded cells treated with $A22^{10}$ are shown. (*B*) A22 alters the localization of EspC-mCherry with and without the β-barrel domain. 0.2% arabinose induced MG1655(p33espCmcherry) (top row) and MG1655(p33tespCmcherry) (bottom row) strains were grown and treated with A22 as described above. Full length EspC-mCherry did not form patchy spirals while truncated EspC-mCherry localized in irregular punctate pattern in A22 treated MG1655. (*C*) The full length EspC-mCherry localization was predominantly bipolar whilst truncated EspC-mCherry was unipolar when produced by the *E. coli* SecA mutant, MM52. Overnight *E. coli*Δ*secA*(p33espCmcherry), *E. coli*Δ*secA*(p33tespCmcherry) and *E. coli*Δ*secA*(p33mcherry) cultures were diluted in LB and induced with 0.02% arabinose. Cultures were grown at 30°C until reaching an OD_{600} of 0.05 (approximately 2 h). Subsequently, the cultures were switched to the non-permissive temperature of 42°C to activate the mutation and imaged after 3 h of incubation. Phase contrast (top row) and confocal mCherry fluorescence microscopy images (bottom row) are shown. The green 555 nm laser was used to detect mCherry. (*D*) Loss of patchy helical localization of FlAsH stained AaaA-TC when produced by the *E. coli* SecA mutant, MM52. Phase contrast, wide field and the more improved contrast and resolution (Deconvolution) of *E. coli*Δ*secA*(p33aaaA-TC) cells show the distinctive bipolar localization of AaaA in absence of Sec translocon. The overnight of *E. coli*Δ*secA*(p33aaaA-TC) was diluted in LB and induced with 0.02% arabinose. Cultures were grown at 30°C until reaching an OD_{600} of 0.05 (approximately 2 h). Subsequently, the cultures were switched to the non-permissive temperature of 42°C to activate the mutation and imaged after 3 h of incubation. Images were taken by confocal microscopy. Scale bars represent 2 µm.

Fig. 6. EspC-mCherry associates with bacterial outer membrane proteins and localizes to a spiral even when produced at low levels. (*A*) MG1655(p33espCmcherry) was induced with 0.02% arabinose for 4 h. A cell lysates was prepared and applied to the bottom of a 32-60% sucrose gradient as described in *Materials and Methods*. Following centrifugation, aliquots from each fraction of the gradient were separated by SDS-PAGE and immunoblotted using α-EspC (top row), the OM control α-TolC (middle row) and the IM control α-AcrB (bottom row). The sucrose concentration (% w/w) in each fraction is shown. Red asterisks indicate the location of the full length EspC-mCherry in the fraction containing 55% sucrose, which aligns to the location of TolC, an OM protein. Molecular weight markers (kDa) are shown. (*B*) Confocal images of *E. coli* cells expressing the full length EspC-mCherry (strain MG1655(p33espCmcherry)) were induced with 0.02% arabinose (top row) or with 0.002% arabinose (bottom row) for 4 h.

Fig. 7. Fluorescence recovery after photobleaching reveals the dynamic nature of the molecules of EspC in patches. The overnight culture of MG1655(p33espCmcherry) (*A*) was diluted 1:100 in fresh LB containing 30 µg/mL Cm and induced with 0.02% arabinose or 4 h at 37°C shaking. Next, the cells were collected and washed with PBS and normalised to OD_{600} of 0.5. 8.0 µl of washed cells were applied to microscopic slides and covered with a coverslip and sealed with transparent nail polish. The overnight culture of

bioRxiv preprint doi: https://doi.org/10.1101/305441; this version posted April 24, 2018. The copyright holder for this preprint (which was not certified by peer review) is the author/funder, who has granted bioRxiv a license to display the preprint in perpetuity. It is made available under aCC-BY-NC-ND 4.0 International license.

MG1655(p33aaaA-TC) (*B*), (used in this experiment as a control), was diluted 1:100 in LB containing 30 µg/mL Cm and grown until OD_{600} of 0.05. Subsequently, the culture was induced by 0.02% arabinose for 2.5 h. Cells were prepared for FlAsH staining following the protocol described in *Materials and Methods*and subjected to microscopy as described above. The representative images of EspC-mCherry (*A*) and AaaA-FlAsH (*B*) show fluorescent intensity before and after photobleaching at the region of interest marked by the green circle. Red circles indicate the control unbleached regions. The intensity of fluorescence within the red circles was used as a reference to normalise that within the green circles over time. The Black triangles in graph *C* and *D* show the normalised fluorescent intensity of zones marked by the green circles in each single frame for images in A and B respectively over time.

Supplementary Information

bioRxiv preprint doi: https://doi.org/10.1101/305441; this version posted April 24, 2018. The copyright holder for this preprint (which was not certified by peer review) is the author/funder, who has granted bioRxiv a license to display the preprint in perpetuity. It is made available under aCC-BY-NC-ND 4.0 International license.

Table S1. Bacterial strains used in this study.

Strain	Genotype or Description	Reference
MG1655	*F- λ- ilvG- rfb-50 rph-1.*	(50)
DH5α	F'/*end*A1, *hsd*R17(R- M+), *supE*44, thi-1, recA1, gyrA, relA1, Δ(*lacZYA-argF*) U169, *deoR* [Φ80d *lac*Δ(*lacZ*) M15].	(51)
E. coli Δ*SecA*	*E. coli SecA* mutant MM52 (temperature sensitive mutant).	(52)
E. coli Top10	F- *mcr*A Δ(*mrr-hsd*RMS-*mcr*BC) Φ80*lac*ZΔM15 Δ*lac*X74 *rec*A1 *ara*Δ139 Δ(*ara-leu*)7697 *gal*U *gal*K *rps*L (Str^R) *end*A1 *nup*G	iba company

bioRxiv preprint doi: https://doi.org/10.1101/305441; this version posted April 24, 2018. The copyright holder for this preprint (which was not certified by peer review) is the author/funder, who has granted bioRxiv a license to display the preprint in perpetuity. It is made available under aCC-BY-NC-ND 4.0 International license.

Table S2. Plasmids used in this study.

Plasmid	Description	Construct depiction	Protein size	Antibiotic resistance	Reference
pBAD33	Medium copy number with p15A and F1 ori. Empty vector under the control of an *araBAD* promoter.	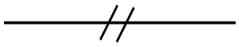	#	Cm^r	Guzman et al 1995
p33espC	pBAD33 containing native *espC* gene under the control of an *araBAD* promoter. Original name pLA33C1	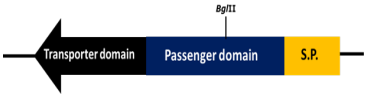	140 kDa	Cm^r	(51)
p33espCmcherry	pBAD33 hosting EspC-mCherry fusion (mCherry was inserted at the *BglII* site approximately in the middle of passenger domain) under the control of an *araBAD* promoter. Original name pLA33C1mc	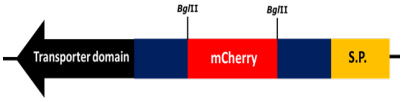	174 kDa	Cm^r	Stephanie Pommier
p33tespCmcherry	pBAD33 containing truncated EspC-mCherry (a stop codon introduced at the end of *mCherry* gene causes a frameshift to truncate translation before the transporter domain) under the control of an *araBAD* promoter. Original name pMAC33.	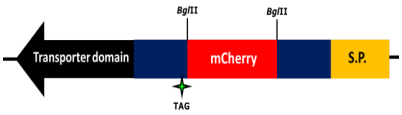	~70 kDa	Cm^r	This study
p33mCherry	pBAD33 containing the *mCherry* gene under the control of an *araBAD* promoter. Original name pLA33mCherry.		~34 kDa	Cm^r	This study
p33espC-TC	p33espC derivative carrying CCPGCC tagged EspC. The TC motif inserted after Gln residue at codon 530 of the espC ORF. Original name pLA33C1-TC.	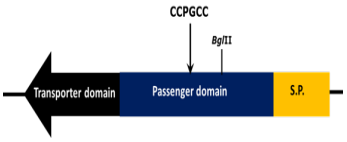	140 kDa	Cm^r	This study
p33aaaA	pBAD33 containing native *aaaA* gene under the control of an *araBAD* promoter. Original name pLA33aaaA.		80 kDa	Cm^r	This study

bioRxiv preprint doi: https://doi.org/10.1101/305441; this version posted April 24, 2018. The copyright holder for this preprint (which was not certified by peer review) is the author/funder, who has granted bioRxiv a license to display the preprint in perpetuity. It is made available under aCC-BY-NC-ND 4.0 International license.

p33aaaA-TC	p33aaaA derivative carrying CCPGCC tagged AaaA. The TC motif inserted after Leu residue at codon 291 of the *aaaA* ORF. Original name pLA33aaaA-TC.	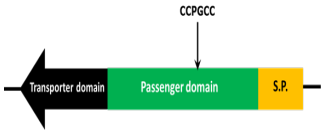	80 kDa	Cm^r	This study
p33taaaA-TC	p33aaaA-TC derivative carrying CCPGCC tagged AaaA, with codon 343 replaced by an amber codon. Original name pLA33aaaATCΔ.	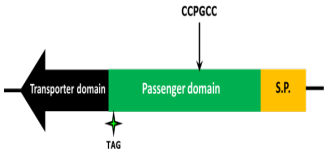	~38 kDa	Cm^r	This study
p33mreB	pBAD33 containing native *mreB* gene under the control of an *araBAD* promoter. Original name pLA33mreB.		~40 kDa	Cm^r	This study
p33mreB-TC	p33mreB derivative carrying CCPGCC tagged MreB. The TC motif inserted after Tyr residue at codon 226 of the *mreB* ORF. Original name pLA33mreB-TC	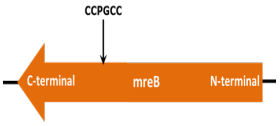	~40 kDa	Cm^r	This study
pmCherry	Prokaryotic expression vector encoding red *mCherry* gene under the control of an *araBAD* promoter.		~34 kDa	Amp^r	Shaner et al 2004

bioRxiv preprint doi: https://doi.org/10.1101/305441; this version posted April 24, 2018. The copyright holder for this preprint (which was not certified by peer review) is the author/funder, who has granted bioRxiv a license to display the preprint in perpetuity. It is made available under aCC-BY-NC-ND 4.0 International license.

Table S3. Oligonucleotide primer sequences used in this study.

Primer Name	Primer Sequence (5`to 3`)	Description
F-*Bgl*II-mCherry	**CT**AGATCT**T***ATG*GTGAGCAAGG GCGAG	Forward primer used to amplify the *mCherry* ORF region with the underlined *Bgl*II restriction site directly upstream of the start codon (italic). The bold nucleotides are additional bases to make mCherry in frame with *espC*. This primer designed by Stephanie Pommier for generating EspC-mCherry fusion.
R-*Bgl*II-mCherry-FL	**AG**AGATCT**AA**CTTGTACAGCTC GTCCAT	Reverse primer used to amplify the *mCherry* ORF region with the underlined *Bgl*II restriction site directly downstream of *mCherry* gene replacing the stop codon. The bold nucleotides are additional bases to make mCherry in frame with *espC*. This primer designed by Stephanie Pommier for generating full length EspC-mCherry fusion.
R-*Bgl*II-mCherry-Δ	**AG**AGATCT**AAA**CTTGTACAGCT CGTCCA	Reverse primer used to amplify the *mCherry* ORF region with the underlined *Bgl*II restriction site directly downstream of *mCherry* gene replacing the stop codon. This primer in particular contains an extra italic bold base to create a frameshift that led to create short EspC-mCherry fusion version (p33tespCmcherry). This primer designed by Stephanie Pommier.
F-*Bgl*II mCherry	**ATA**AGATCT*ATG*GTGAGCAAGG GCGAGGAGGAT	Forward primer used to amplify the *mCherry* ORF region with the underlined *Bgl*II restriction site directly upstream of the ATG start codon (italic). The bold nucleotides are additional bases to ensure accurate *Bgl*II restriction site digestion. This primer used to create pLA33mChery vector.
R-*Sal*I mCherry	**TAT**GTCGACCTTGTACAGCTCG TCCATGCCGCCG	Reverse primer used to amplify the *mCherry* ORF region with the underlined *Sal*II restriction site directly downstream of *mCherry* gene. The bold nucleotides are additional bases to ensure accurate *Bgl*II restriction site digestion. Please note that the stop codon was autonomously introduced downstream the restriction site.

bioRxiv preprint doi: https://doi.org/10.1101/305441; this version posted April 24, 2018. The copyright holder for this preprint (which was not certified by peer review) is the author/funder, who has granted bioRxiv a license to display the preprint in perpetuity. It is made available under aCC-BY-NC-ND 4.0 International license.

		This primer used to create p33mcherry vector.
F-MreB-*Bgl*II	**TAT**AGATCT*ATG*TTGAAAAAATT TCGTGGCAT	Forward primer used to amplify the *mreB* ORF region with the underlined *Bgl*II restriction site directly upstream of the ATG start codon (italic). The bold nucleotides are additional bases to ensure accurate *Bgl*II restriction site digestion.
R-MreB-*Sal*I	**ATA**GTCGAC*TTA*CTCTTCGCTGA ACAGGTC	Reverse primer used to amplify the *mreB* ORF region with the underlined *Sal*I restriction site directly downstream of TAA stop codon (italic). The bold nucleotides are additional bases to ensure accurate *Sal*I restriction site digestion.
F-MreB CCXXCC	TCGGTTCGGCTTAT**TGTTGC**CC GGGC**TGTTGC**GATGAAGTCCGT GAAAT	Forward primer used to amplify p33mreB plasmid for encoding the *mreB* ORF region with the bold codons to generate the optimal CCPGCC motif. XX are representing Pro-227–Gly228 residues.
R-MreB CCXXCC	ATTTCACGGACTTCATC**GCAAC A**GCCCGG**GCAACA**ATAAGCCG AACCGA	Reverse primer used to amplify p33mreB plasmid for encoding the *mreB* ORF region with the bold codons to generate the optimal CCPGCC motif. XX are representing Pro-227–Gly228 residues.
F-EspC CCPGCC	CAGAGATAAACCACCAG**TGCTG TCCAGGCTGCTGC**TTTGATACC CAAAAAAATAATAGTCGC	Forward primer used to amplify p33espC plasmid for encoding the *espC* ORF region with the bold codons to generate the optimal CCPGCC motif. This motif sequence is inserted between Gln-530 and Phe-531 residues.
R-EspC CCPGCC	GCGACTATTATTTTTTGGGTAT CAAA**GCAGCAGCCTGGACAGC A**CTGGTGGTTTATCTCTG	Reverse primer used to amplify p33espC plasmid for encoding the *espC* ORF region with the bold codons to generate the optimal CCPGCC motif. This motif sequence is inserted between Gln-530 and Phe-531 residues.
F-AaaA CCPXCC	AGTACTGACCAACGCCCTC**TGC TGTCCA**GGC**TGCTGC**CAGGAG CGCATCGAGC	Forward primer used to amplify p33aaaA plasmid for encoding the *aaaA* ORF region with the bold codons to generate the optimal CCPGCC motif. X is representing Gly-292 residue.
R-AaaA CCPXCC	GCTCGATGCGCTCCTG**GCAGCA** GCC**TGGACAGCA**GAGGGCGTT GGTCAGTACT	Reverse primer used to amplify p33aaaA plasmid for encoding the *aaaA ORF* region with the bold codons to generate the optimal CCPGCC motif. X is representing Gly-292 residue.

bioRxiv preprint doi: https://doi.org/10.1101/305441; this version posted April 24, 2018. The copyright holder for this preprint (which was not certified by peer review) is the author/funder, who has granted bioRxiv a license to display the preprint in perpetuity. It is made available under aCC-BY-NC-ND 4.0 International license.

F-AaaATAG343	ATGGAAGACCAGTTG**TAG**CGCC AGCATCAGGCACT	Forward primer used to amplify p33aaaA-TC plasmid for encoding the *aaaA* ORF region with the bold amber stop codon at aa positon 343. The underlined bold nucleotide is representing the changed base that required for the mutation.
R-AaaATAG343	AGTGCCTGATGCTGGCG**CTA**CA ACTGGTCTTCCAT	Reverse primer used to amplify p33aaaA-TC plasmid for encoding the *aaaA* ORF region with the black bold amber stop codon at aa positon 343. The underlined bold nucleotide is representing the changed base that required for the mutation.
Primers for sequencing		
espCFNO1	GATCTGGTGATAAAAACATTA	Primer to sequence *espC* (51).
espCF12	AAGTTTGTTGTTGAAACA	Primer to sequence *espC* (51).
mCherry MA-F MID	TCCCCGACTACTTGAAGCTG	Primer to sequence *mCherry*.
pLADCBP3f	TTAGAGAGGGTGGGGGTTACCT GCATGCTGC	Primer to sequence *espC* (51).
Primer MA2-F	GAAACAGGAGTATTACTCCC	Primer to sequence *mCherry*.
espCKHf1	GAACAAGCGTATGGGTGA	Primer to sequence *espC* (51).
AaaA upstream F1	CACGGCGTCACACTTTGCTATGC CA	Primer to sequence *aaaA*.
AaaA-F2	GGTTCGCGTGCCTACGTCGAGT CCCT	Primer to sequence *aaaA*.
AaaA-F3	GTTTCGACATGCCTGGCAATCC GG	Primer to sequence *aaaA*.
AaaA-F4	GACATGGGCGGCGTGGACAAG GATTTCG	Primer to sequence *aaaA*.
MreB-F2	TGGTACCACTGAAGTTGCTGTTA T	Primer to sequence *mreB*.

Fig. S1. Strategy for inserting fluorescent tags into the EspC passenger domain. (*A*) Using mCherry fluorescent protein as a tag. (*i*) The native 140 kDa EspC protein is shown with the relative position of the *Bgl*II restriction site on its encoding DNA. (*ii*) Digestion of the DNA template by *Bgl*II opened *espC*. Ligation to a DNA fragment (encoding the 34 kDa mCherry protein) which had been digested by the same enzyme was then undertaken (*iii*). (*iv*) Successful insertion of the fluorescent mCherry protein into passenger domain results in formation of full length 174 kDa EspC-mCherry protein. (*B*)

bioRxiv preprint doi: https://doi.org/10.1101/305441; this version posted April 24, 2018. The copyright holder for this preprint (which was not certified by peer review) is the author/funder, who has granted bioRxiv a license to display the preprint in perpetuity. It is made available under aCC-BY-NC-ND 4.0 International license.

Using FlAsH-tag technology. The position selected for CCPGCC motif insertion on the predicted native EspC passenger domain structure. The 3D model of EspC passenger domain developed in PyMol Zalman software showing the location of residues on external loops selected for creating the CCPGCC motif. The catalytic serine residue at position 256 hosted in motif GDSGS is highlighted in red.

Fig. S2. Cloning strategy to produce mCherry under the control of arabinose. (*A*) Plasmid p33espC harbouring *espC* in pBAD33 was subjected to site directed mutagenesis using primers F-p33espC-*Bgl*II/R-p33espC-*Bgl*II to insert a *Bgl*II restriction site downstream of the arabinose promoter. Successful mutagenic PCR was revealed by the expected sized DNA product ~9293 bp (undigested as a control and digested with *Dpn*I restriction enzyme). (*B*) Confirmation of the new construct (p33espC*Bgl*II) was achieved through a single digestion using *Bgl*II. Digested p33espC (1) is shown alongside p33esp*Bgl*II (2) revealing the generation of second DNA fragment ~1000 bp in lane 2. To enable cloning *mCherry* gene, p33espC*Bgl*II was digested with *Bgl*II and *Sal*I enzymes (Agarose B, lane 4**)** alongside the control p33espC (Agarose B, lane 3). NB: Introduction of the second *Bgl*II site caused production of four DNA fragments, two of which were very similar ~1101 bp and ~1064 bp (red asterisks) (Agarose B, lane 4). (*C*) The opened pBAD33 vector generated from p33espC*Bgl*II was ligated to the similarly digested PCR product bearing *mCherry* to yield p33mcherry. The new construct was verified by sequencing and by digestion with restriction enzymes. Lane 1: pBAD33 vector digested with *Bgl*II and *Sal*I enzymes (control), Lane 2: similarly digested PCR product bearing mCherry, Lane 3: undigested p33mcherry, Lane 4: p33mcherry digested with only *Sal*I, Lane 5: p33mcherry digested with *Bgl*II, Lane 6: p33mcherry digested with both *Bgl*II and *Sal*I. All DNA samples were separated through 0.8% agarose gel alongside 1 kb DNA ladder.

Fig. S3. FlAsH addition does not generate obvious staining in the absence of an AT with a TC-motif. Controls MG1655 wt (*A*) and MG1655(pBAD33) (*B*) were grown, induced and exposed to exogenous FIAsH substrate as described in Fig. 3.

Fig. S4. Strategy for inserting fluorescent tags into AaaA. (*A*) a 2065 bp DNA fragment containing the *aaaA* gene was released by digestion of pET21(a+)::aaaA with *Bgl*II and *Sal*I (lane 1). The *aaaA* DNA fragment was ligated into 5327 bp open pBAD33 vector. (*B*) The pBad33 backbone was generated by digestion of pLA33C1*Bgl*II with *Bgl*II and *Sal*I (lane 1). The confirmation of the new construct (p33aaaA) was achieved by DNA sequencing or as shown in (*C*) via digestion with either (i) *Bgl*II (lanes 1, 2, and 3 digestion of p33espC, pLA33C1*Bgl*II and p33aaaA respectively: note that a fragment of ~1064 bp represents the upstream portion of *espC* released in lane 2), or (ii) with *Bgl*II and *Sal*I (pLA33C1*Bgl*II and p33aaaA plasmids lanes 4 and 5 respectively). DNA fragment sizes were estimated by comparison to the 1kb DNA ladder (lanes labelled M) and control undigested plasmids (C, C4 and C5).

Fig. S5. Cloning strategy to remove β-barrel and generate fluorescently labelled, truncated EspC. (*A*) p33espCmcherry and p18tespCmcherry were digested with *Sac*I and *Hind*III. As expected, p33espCmcherry digestion yielded the first target fragment of approximately 5.3 kb comprising the pBAD33 vector (white asterisks) in addition to the ~4.6 kb full length EspC-mCherry. It was not possible to differentiate the separate digested products of p18tespCmcherry due to the size similarity between the pBAD18 vector (~4.6 kb) and truncated EspC-mCherry (~4.6 kb) products. (*B*) To enable separation of vector and insert DNA on agarose gel electrophoresis, pMAC18-75 was further digested with *Nde*I to produce two smaller fragments. (*C*) The confirmation of the new p33tespCmcherry construct was via *Sac*I/*Hin*dIII digestion. Two different colonies containing p33tespCmcherry were evaluated 1 & 2 (with (D) and without (C) digestion) alongside the controls;

bioRxiv preprint doi: https://doi.org/10.1101/305441; this version posted April 24, 2018. The copyright holder for this preprint (which was not certified by peer review) is the author/funder, who has granted bioRxiv a license to display the preprint in perpetuity. It is made available under aCC-BY-NC-ND 4.0 International license.

open pBAD33 vector and *Sac*I/*Hin*dIII digested truncated EspC-mCherry. All DNA samples are separated through 0.8% agarose gel alongside the DNA ladder.

Fig. S6. *E. coli* producing FlAsH stained truncated AaaA-TC display a dense random distribution of fluorescent spots with no obvious helical arrangement. MG1655(p33taaaA-TC) was grown and imaged as described in Fig. 3, and the 3D rendering of structured illumination images are shown (Movie S4).

Fig. S7. Strategy to fluorescently label MreB-mCherry. (*A*) The open reading frame of *mreB* was PCR amplified to incorporate *Bgl*II and *Sal*I restriction sites at the 5' and 3' ends. The expected ~1044 bp PCR product confirmed the successful amplification. (*B*) The PCR product was digested with *Bgl*II and *Sal*I and ligated into pBAD33 vector which had been digested with the same enzymes. (*C*) p33mreB was digested with the same set of enzymes to confirm this by yielding the expected digestion profile (5327 bp plus 1044 bp fragments). Lane: C1 and C2 show the controls of only open pBAD33 vector and digested *mreB* fragment respectively, Lane 1: single B*gl*II digestion, Lane 2: *Bgl*II and *Sal*I digestion. To generate p33mreB (*D*) To enable insertion of mCherry into MreB, site directed mutagenesis was first utilized to introduce a *Avr*II restriction site to yielding pLA33mreBAvrII. Lane C: undigested control, Lane 1: *Dpn*I digested PCR products. (*F*) mCherry gene was amplified using primers designed to include *Avr*II restriction site at both gene ends. (*E*) This mCherry PCR product was digested with *Avr*II and ligated into open pLA33mreBAvrII which had been digested with the same restriction enzyme (Lane C: control undigested plasmid DNA, Lane 1: expected open vector after digestion with *Avr*II enzyme). (*G*) The new construct (pLA33mreBmc) was successfully made and verified by single *Sal*I and *Avr*II digestion and comparison with similarly digested pLA33mreBAvrII vector (pLA33mreBAvrII is shown in Lane 1: undigested, Lane 2: digested with *Sal*I, Lane 3: digested with *Avr*II. pLA33mreBmc is shown Lane 4: undigested, Lane 5: digested with *Sal*I, Lane 6: digested with *Avr*II). M indicates the 1 kb DNA molecular marker. Site directed mutagenesis was performed on p33mreB to engineer *mreB* to encode two cysteine residues before and after residues Pro227–Gly228 using site-directed mutagenesis (p33mreB-TC).

Fig. S8. The full length EspC-mCherry is associated with the bacterial outer membrane when induced by high levels of arabinose. (*A*) The control MG1655(pBAD33) and (*B*) MG1655(p33espCmcherry) were induced with either 0.02% or 0.2% arabinose respectivelyfor 4 h. Cell lysates were prepared and applied to applied to the bottom of a 33.5-61% sucrose gradient. The sucrose concentration (% w/w) in each fraction collected following centrifugation is shown. Aliquots from each fraction of the gradient were separated by SDS-PAGE and immunoblotted using α-EspC (top row), the OM control α-TolC (middle row) and the IM control α-AcrB (bottom row). Red asterisks indicate the location of the full length EspC-mCherry in the fraction containing 54.5% sucrose, which aligns to the location of TolC, an OM protein (A). No EspC was found in the control MG1655(pBAD33) strain (B). Molecular weight markers (kDa) are shown.

Fig. S9. Cartoon of potential AT localization pathway. The Sec translocon (blue circles) and MreB filaments (magenta linked circles) are shown distributed along the cell in a helix and anchored to the inner membrane by proteins (grey/black ovals). Periplasmic proteins e.g. chaperones are indicated as grey circles and Outer membrane (OM) located BAM or Tam complexes by the green barrels. In orange precursor ATs are sown make on the ribosome (black dumbbell) in the cytoplasm as an unfolded precursor (*A*) that would be ushered by chaperones to the Sec translocon via its amino terminal signal peptide (*B*). We speculate that during inner membrane (IM) translocation using Sec that the AT is dynamically moving along the cytoskeleton towards the bacterial poles (*C*). This could be energetically driven by the treadmilling of the divisome (e.g. FtsZ at the centre of the cell), or by MreB filament assembly and disassembly, as indicated by the orange arrows. As IM translocation occurs, the signal peptide will be cleaved off and the remainder of the AT will dock with BAM/TAM and be secreted. Finally (*D*), the folded β-barrel will be inserted into the OM (orange

bioRxiv preprint doi: https://doi.org/10.1101/305441; this version posted April 24, 2018. The copyright holder for this preprint (which was not certified by peer review) is the author/funder, who has granted bioRxiv a license to display the preprint in perpetuity. It is made available under aCC-BY-NC-ND 4.0 International license.

barrel), although this may not be exclusively at the poles. For AaaA: the passenger protease domain would remain attached to the β-barrel, folded and extracellular. For EspC: autoproteolysis would release the folded passenger protease to the extracellular milieu.

Fig. S10. *E. coli* MG1655 carrying plasmids encoding EspC or AaaA produce equivalent quantities of autotransporters at the predicted size. Panel *A*: Strains encoding native EspC (MG1655(p33espC), blue asterisk 140 kDa), EspC-mCherry (MG1655(p33espCmcherry), yellow asterisk 174 kDa) or tEspC-mCherry (MG1655(p33tespCmcherry), red asterisk 70 kDa) were applied to SDS-PAGE alongside a control producing native mCherry (MG1655(pmCherry), green asterisk 30 kDa). The left panel was immunoblotted with anti-EspC, and the right with anti-dsRed. Panel *B*. Strains producing native AaaA (MG1655(pLAC33aaaA) pink asterisk 70 kDa), AaaA with the FlAsH motif (MG1655(pLAC33aaaA-TC) orange asterisk 70 kDa) and AaaA with the FlAsH motif and truncated before the β-barrel (MG1655(pLAC33aaaA-TCΔ) black asterisk 38 kDa). Immunoblotting was performed with anti-AaaA, and an extract from cells producing tEspC-mCherry (MG1655(p33tespCmcherry)) was applied alongside as a negative control. Strains were grown and induced with arabinose and whole cell extracts were applied to SDS-PAGE and immunoblotted as detailed in materials and methods alongside molecular weight markers with the sizes indicated in kDa.

Fig. S11. Activity of AaaA is retained by the mutant forms used in this study. (*A*). MG1655 carrying the empty vector pBAD33 (×), p33aaaA (■), p33aaaA-TC (▲) and p33aaaA^{C233S} (●) were grown in LB medium containing 30 µg/ml Cm overnight at 37℃ shaking. Next day, cells were resuspended in fresh LB medium (1:100) containing similar amounts of antibiotic and incubated until reaching OD_{600} of 0.05. Following the induction period of 2.5 h with 0.02% arabinose, cells were collected for the p-nitroanalide assay. Cells were washed, resuspended in MMP and normalised to OD_{600} of 0.25. Subsequently, cells were mixed with arginine-p-nitroanilide (1 mM), and moved to clear bottomed 96 well plate to be monitored in Lucy Plate Reader (405 nm) at 37℃ for 12 h. (*B*) MG1655 carrying the empty vector pBAD33 (×), p33aaaA (■), p33aaaA-TC (▲) and p33taaaA-TC (expressing truncated TC-tagged AaaA without β-barrel domain) (●) were grown were analysed as described for panel (*A*). These experiments were performed in triplicate and error bars indicate the standard deviation.

Movie S1. Animation of individual confocal sections reveal the extended helical patterns along the length of the bacterium (See Fig. 1*C*).

Movie S2. Animation of 3D rendering of structured illumination images reveal the patchy helical localization of FlAsH labelled TC-tagged EspC within the cell envelope (See Fig. 2C).

Movie S3. Animation of 3D rendering of structured illumination images reveal the spiral localization of FlAsH labelled AaaA-TC within the cell envelope. (See Fig. 3D).

Movie S4. Animation of 3D rendering of structured illumination images reveal a dense random distribution of fluorescent spots with no structured helical arrangement of FlAsH stained truncated AaaA-TC (see Fig. S6).

Fig. 1

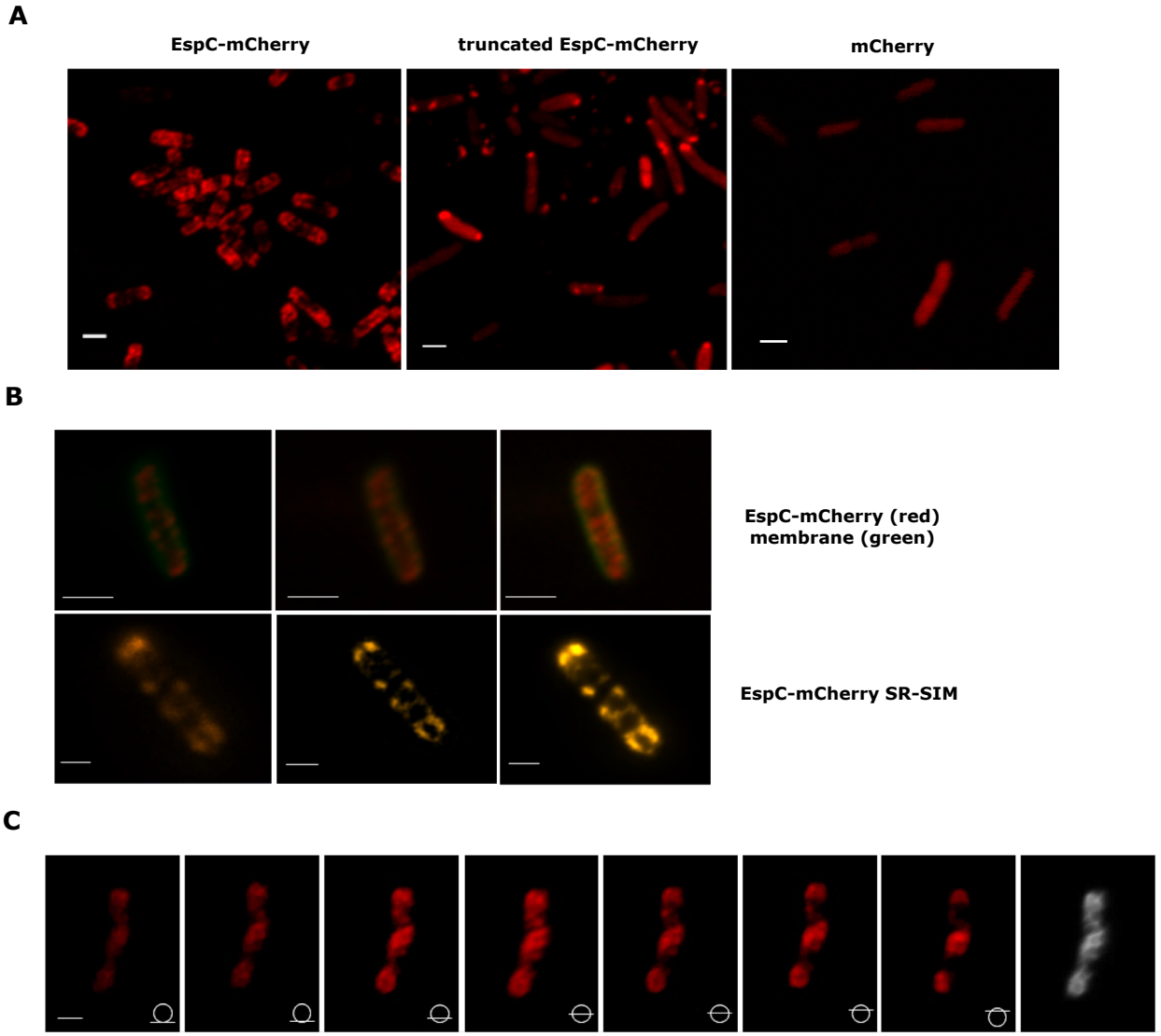
A
EspC-mCherry
truncated EspC-mCherry
mCherry
B
EspC-mCherry (red)
membrane (green)
EspC-mCherry SR-SIM
C

Fig. 2

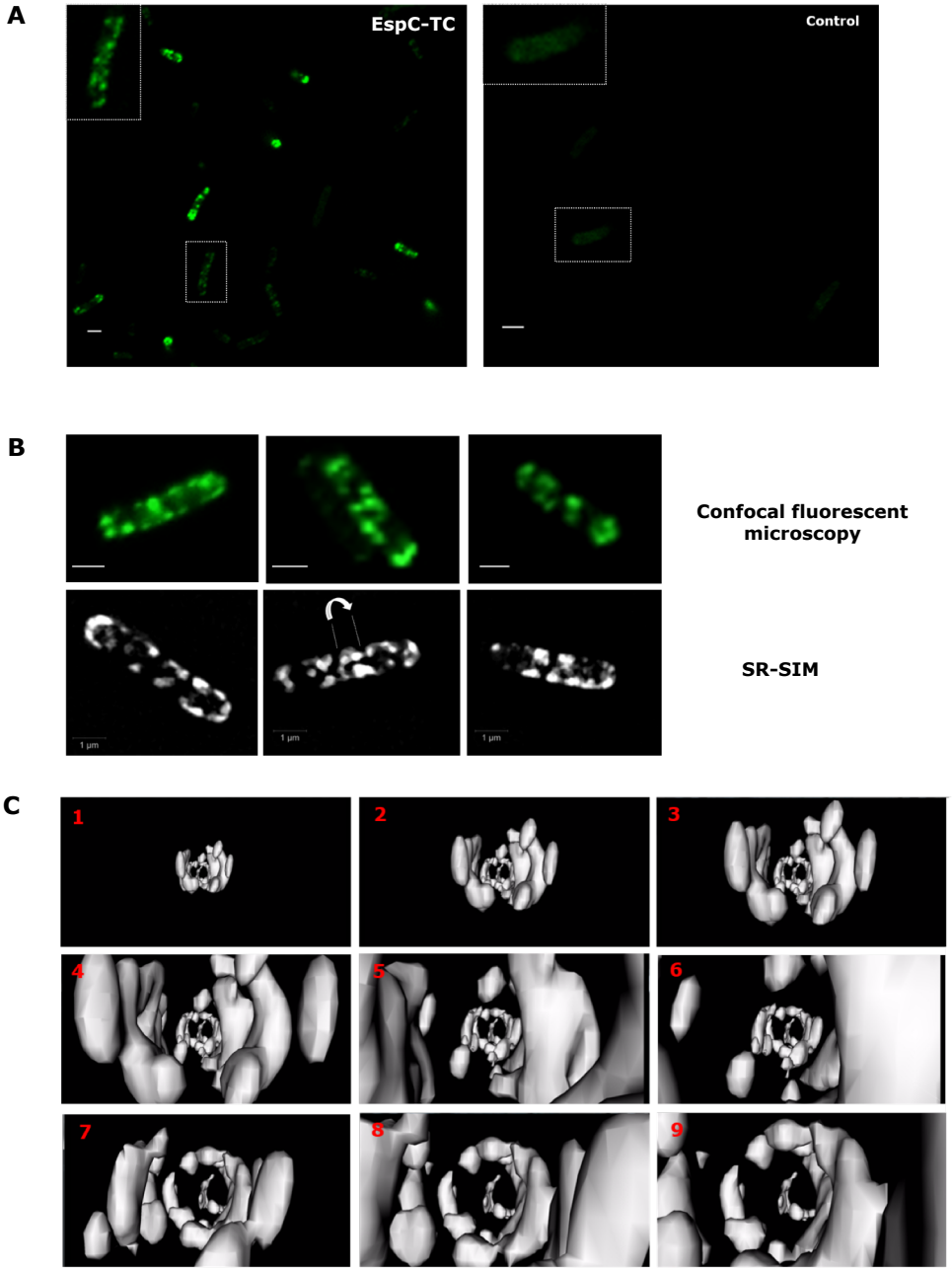
A
EspC-TC
Control
B
Confocal fluorescent microscopy
SR-SIM
1 μm
1 μm
1 μm
C
1
2
3
4
5
6
7
8
9

Fig. 3

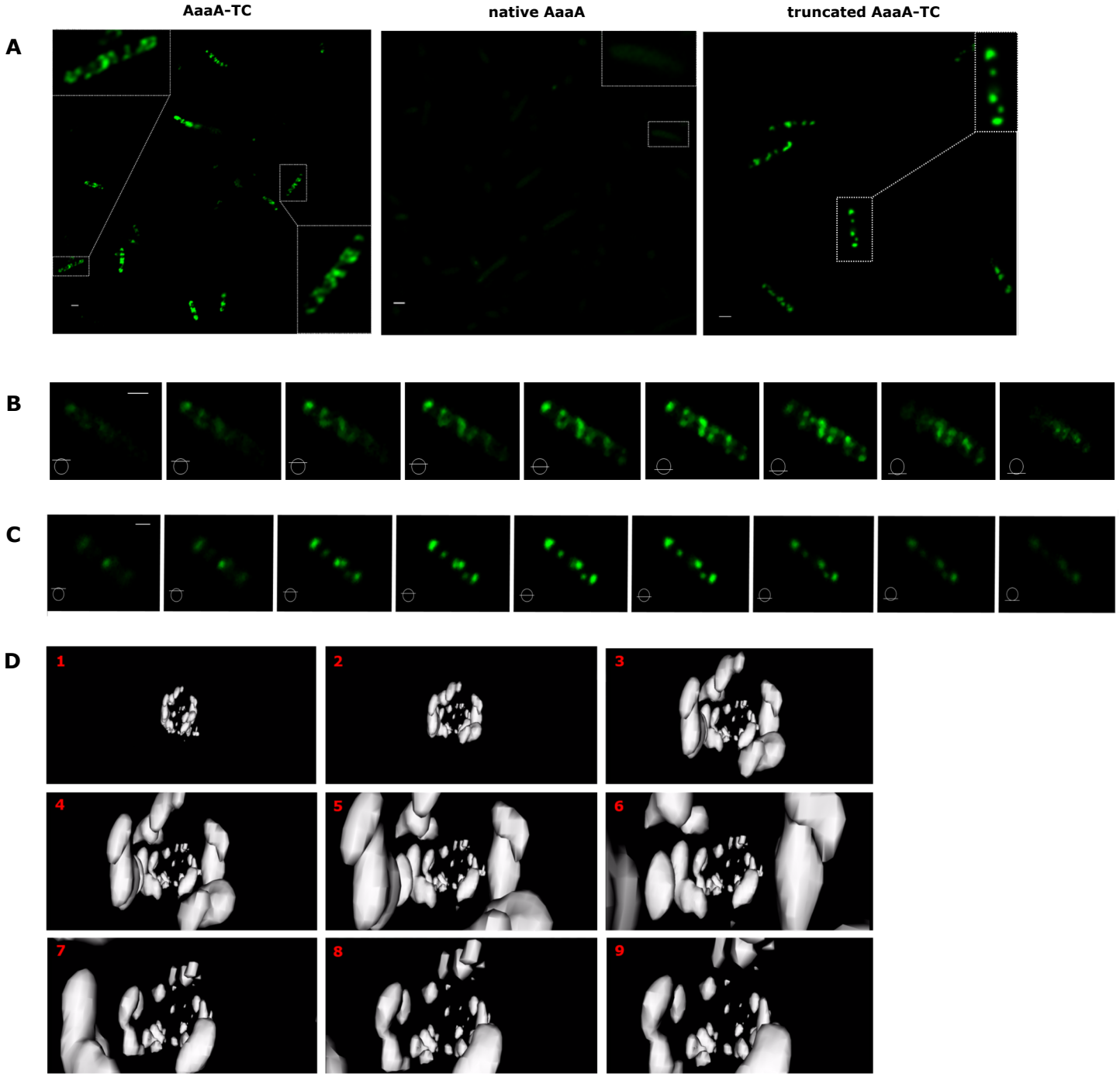

Fig. 4

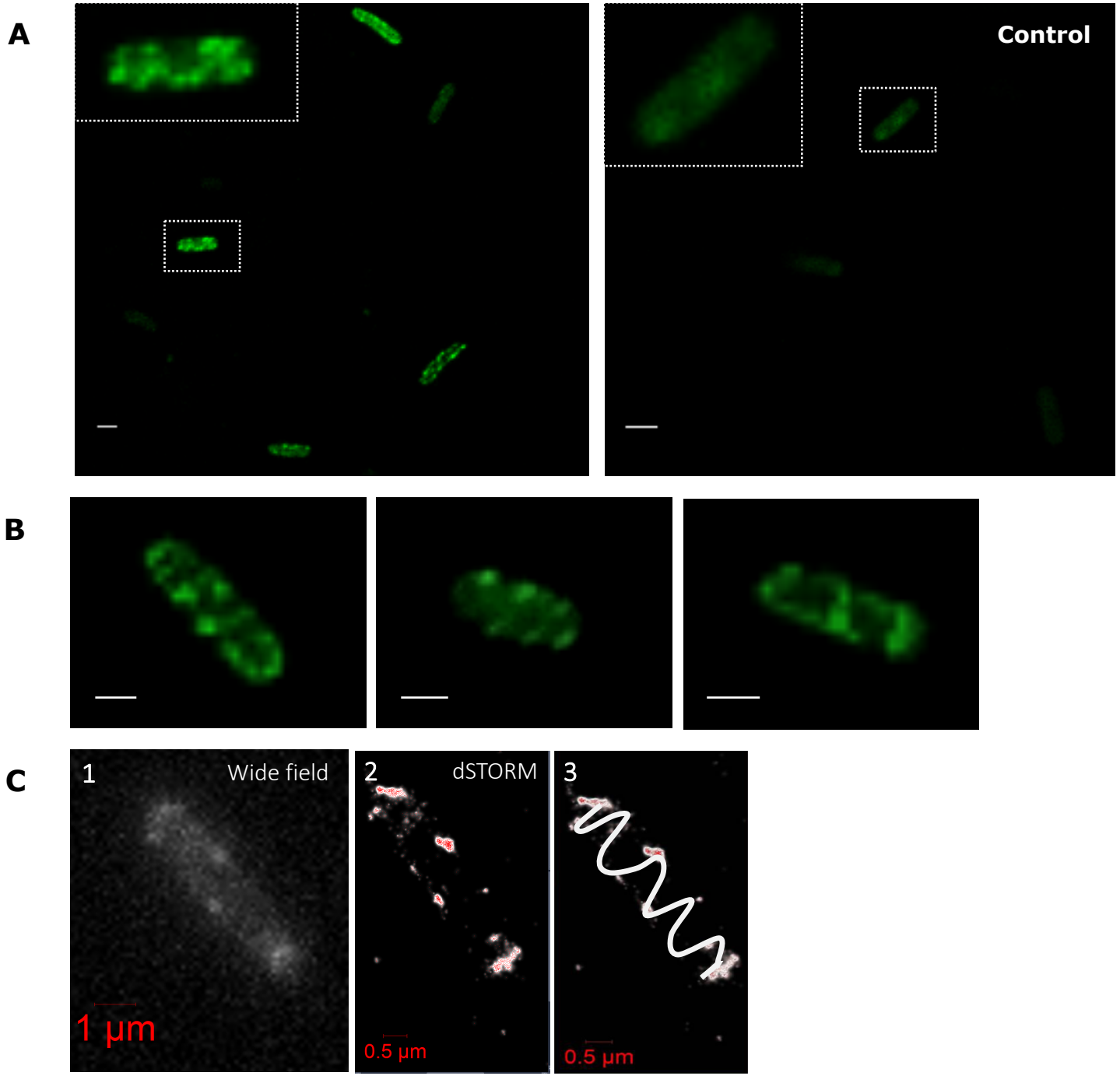

Fig. 5

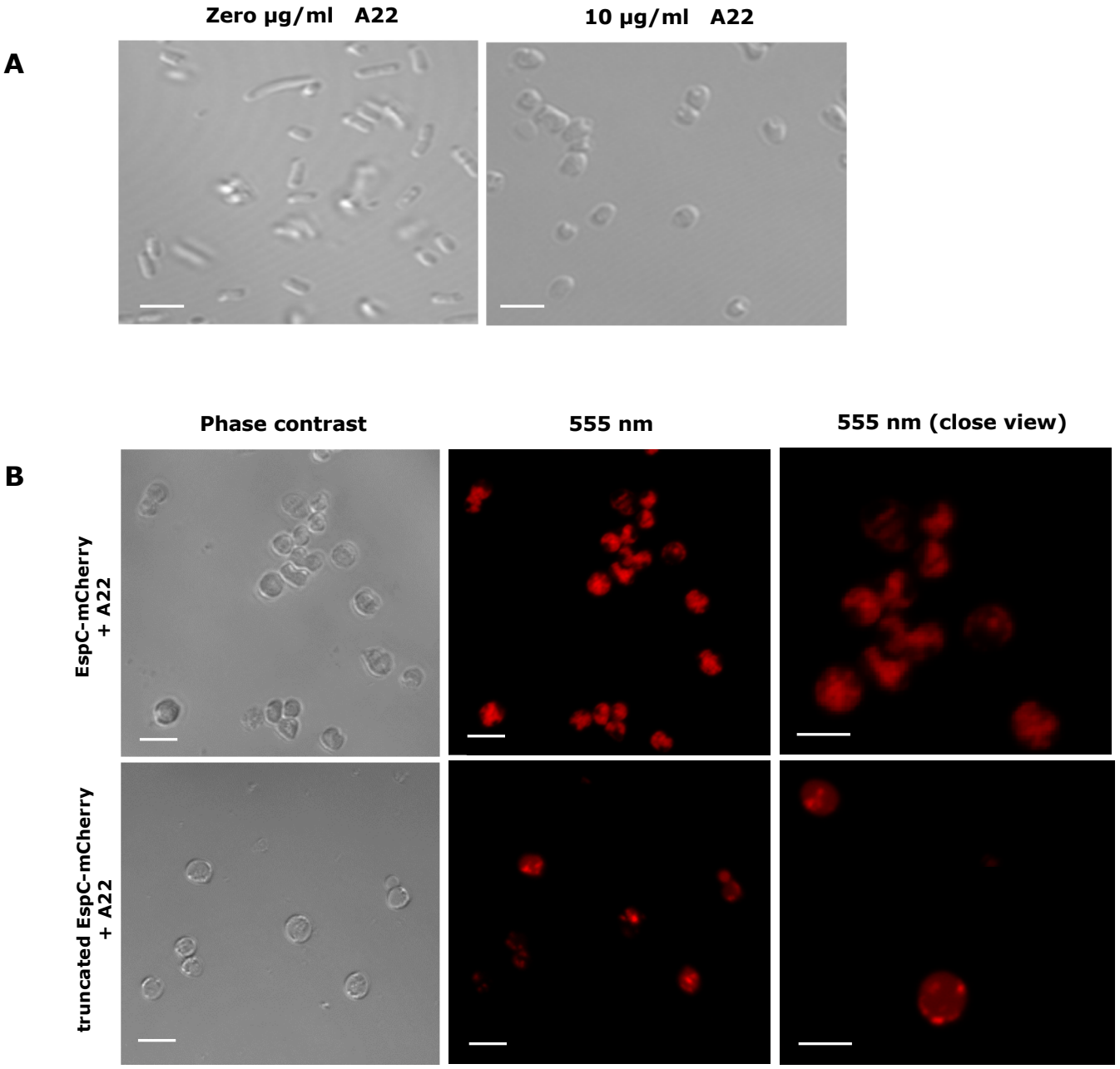
A
Zero µg/ml A22
10 µg/ml A22
B
Phase contrast
555 nm
555 nm (close view)
EspC-mCherry + A22
truncated EspC-mCherry + A22

Fig. 5

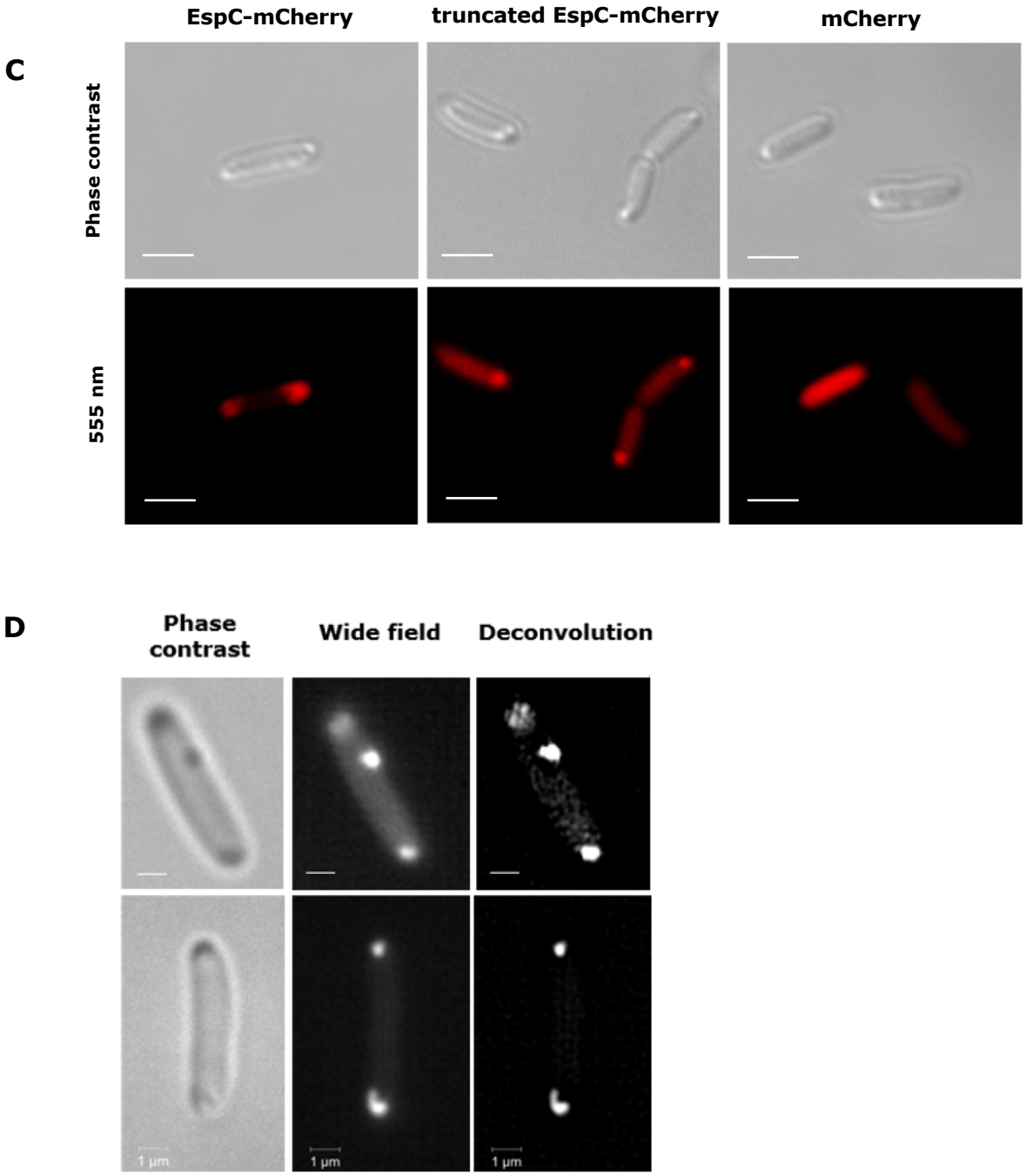
C
EspC-mCherry
truncated EspC-mCherry
mCherry
Phase contrast
555 nm
D
Phase contrast
Wide field
Deconvolution
1 µm
1 µm
1 µm

Fig. 6

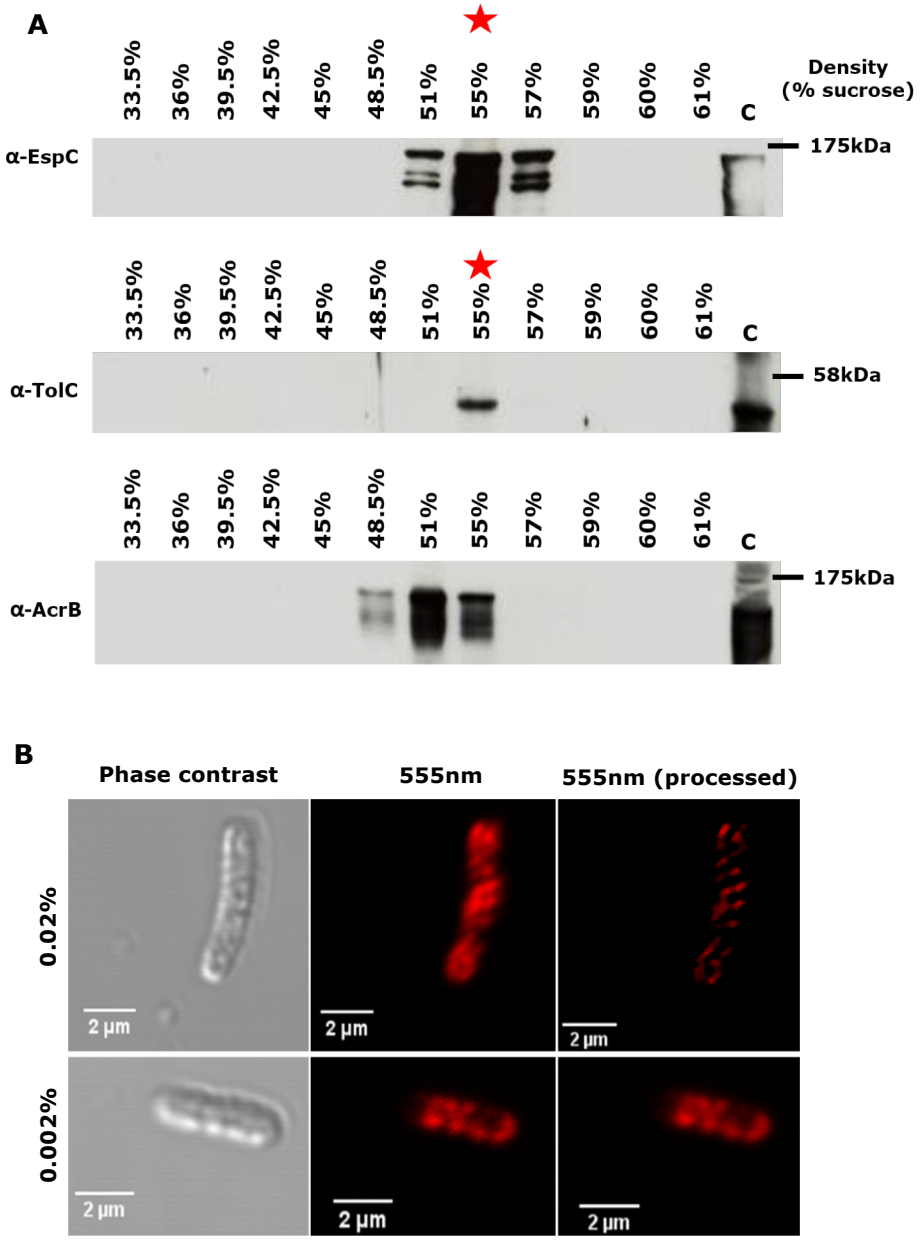
A
33.5%
36%
39.5%
42.5%
45%
48.5%
51%
55%
57%
59%
60%
61%
C
Density
(% sucrose)
α-EspC
175kDa
α-TolC
58kDa
α-AcrB
175kDa
B
Phase contrast
555nm
555nm (processed)
0.02%
0.002%
2 µm

Fig. 7

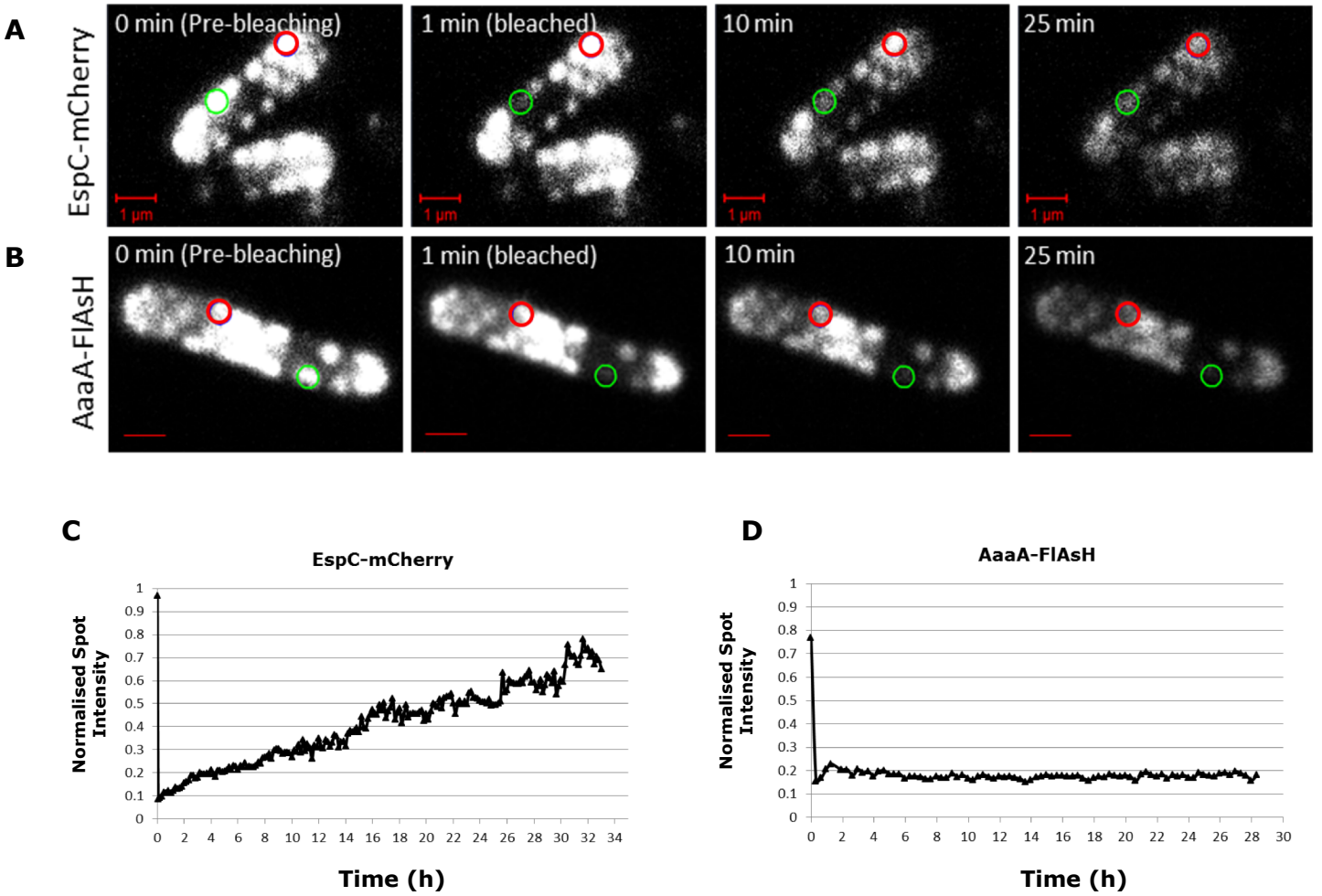
A
EspC-mCherry
0 min (Pre-bleaching)
1 min (bleached)
10 min
25 min
1 µm
B
AaaA-FlAsH
0 min (Pre-bleaching)
1 min (bleached)
10 min
25 min
C
EspC-mCherry
Normalised Spot Intensity
Time (h)
D
AaaA-FlAsH
Normalised Spot Intensity
Time (h)